COMPARISON OF EQUIVALENT DIAMETER END MILL MODELS FOR DYNAMICS PREDICTION BY RECEPTANCE COUPLING SUBSTRUCTURE ANALYSIS

By

UTTARA VIJAY KUMAR

A THESIS PRESENTED TO THE GRADUATE SCHOOL
OF THE UNIVERSITY OF FLORIDA IN PARTIAL FULFILLMENT
OF THE REQUIREMENTS FOR THE DEGREE OF
MASTER OF SCIENCE

UNIVERSITY OF FLORIDA

2009

To my parents, Alka and Vijay Kantute

ACKNOWLEDGMENTS

I want to thank my parents for their immense love, encouragement and for the principles and values they have instilled in me. I would also like to thank my sister, Shweta, who has been my best friend and my brother-in-law, Shwetal, for their care and constant motivation.

I extend my sincere gratitude to my advisor, Dr. Tony L. Schmitz, a mentor in every sense of the word, for his guidance and exceptional ideas throughout my research. I feel privileged to have had the opportunity to interact with two distinguished yet so humble personalities, my committee members, Dr. Schueller and Dr. Greenslet. I am grateful to Dr. Cristescu, who has been a father-like figure to me.

I thank my colleagues in the Machine Tool Research Center (MTRC) for their help, support and sense of humor, making the MTRC a fun place to work. I am also thankful to all my friends in Gainesville especially, Ashwin Dani, for being a pillar of strength.

TABLE OF CONTENTS

APPENDIX

LIST OF TABLES

LIST OF FIGURES

Abstract of Thesis Presented to the Graduate School
of the University of Florida in Partial Fulfillment of the
Requirements for the Degree of Master of Science

COMPARISON OF EQUIVALENT DIAMETER END MILL MODELS FOR DYNAMICS PREDICTION BY RECEPTANCE COUPLING SUBSTRUCTURE ANALYSIS

By

Uttara Vijay Kumar

December 2009

Chair: Tony L. Schmitz
Major: Mechanical Engineering

With the increase in the spindle speeds made available by new spindle designs coupled with higher machine velocities and accelerations, the knowledge of tool-holder-spindle-machine dynamics becomes all the more important if the improved machine capabilities are to be exploited. The wider acceptance of Receptance Coupling Substructure Analysis (RCSA) in the field of high speed machining to predict the tool point dynamics emphasizes the need to develop tool-holder models that can accurately predict the dynamics of a particular machine to determine the best spindle speed and corresponding material removal rate (MRR). This thesis describes an investigation of tool models that are required as part of the RCSA tool-holder-spindle-machine coupling procedure.

Finite element analysis (FEA) is used to approximate the tool's cross-sectional geometry and generate frequency response functions which represent the free-free beam's behavior. Because FEA is computationally expensive, alternative models using equivalent diameters for the fluted portion are also considered. In this work three methods are applied in order to calculate the equivalent diameter of the fluted portion of the end mill. The aim of this work is to compare these methods for equivalent diameter selection and select the best alternative. The prediction of

frequency response function (FRF) using the equivalent diameter models of the fluted end mill are compared to FRF measurements obtained using impact testing.

CHAPTER 1
INTRODUCTION

Research Description

The process dynamics during milling can dramatically affect productivity due to unstable cutting conditions (or chatter) and forced vibrations which can cause part geometry errors (or surface location errors) [1-3]. Modeling these process dynamics requires knowledge of the structural dynamics of the cutting system, particularly the response of the tool-holder-spindle-machine assembly (as reflected at the tool point). With the increase in the spindle speeds made available by new spindle designs coupled with higher machine velocities and accelerations, the knowledge of tool-holder-spindle-machine dynamics becomes indispensable if the improved machine capabilities are to be exploited. Efforts are continuously being made to develop methods that accurately predict the dynamics of a particular machine to determine the best spindle speed and material removal rate (MRR) with a minimal number of tests.

The prediction of tool point dynamics using Receptance Coupling Substructure Analysis (RCSA) [4] is gaining wider acceptance in the field of high speed machining. The analytical RCSA method is applied to join models of the tool and holder with a measurement of the spindle-machine. This thesis describes an investigation of tool models that are required as part of the RCSA tool-holder-spindle-machine coupling procedure. Finite element analysis (FEA) is used to approximate the tool's cross-sectional geometry and generate frequency response functions which represent the free-free beam's behavior. Because FEA is computationally expensive, alternative models are also considered. In a study by Kops and Vo [5], the fluted portion was approximated as a uniform beam by determining an equivalent diameter based on FEA and beam equations were used for deflection calculations. Schmitz *et al.* also made use of the equivalent diameter approach [4, 6-7]. Three methods are applied in this work to calculate

the equivalent diameter of the fluted portion of the end mill: 1) the area of the cross-section of the end mill's fluted area; 2) the area moment of inertia of the cross-section of the end mill's fluted area; and 3) and the mass of the end mill. The goal of this work is to compare these methods for equivalent diameter selection and identify the best alternative. The results of frequency response function (FRF) measurements are compared to prediction using the equivalent diameter models of the fluted end mill.

Literature Review

Many attempts have been made to model the milling process and it continues to be a widely studied topic. The time marching numerical integration approach to model the milling process is summarized by Smith and Tlusty [8]. Related work includes the mechanistic model approach for the prediction of the force system [9]. Frequency domain solutions have been applied to determine process stability in the form of stability lobe diagrams, which identify stable and unstable cutting zones as a function of axial depth of cut and spindle speed [10]. Altintas and Budak used a Fourier series (frequency domain) approach to approximate the time varying cutting force coefficients for stability lobe diagram development [11]. A closed form, frequency domain solution for surface location error in milling was developed by Schmitz and Mann [12]. A numerical method for the stability analysis of linear time-delayed system based on a semi-discretization technique was developed [13]. Modeling approaches based on finite element analysis [14] and, later, time finite element analysis [15] have also been developed. In all the modeling methods, a description of the system dynamic response comprised of the tool-holder-spindle-machine assembly receptance is required. This response can be obtained on a case-by-case basis via impact testing, where an instrumented hammer is used to excite the tool point and the response is measured using (typically) a low-mass accelerometer. However, because each tool-holder combination must be measured on each machine, the number of experiments can be

excessive. Therefore, the preferred method is application of an appropriate modeling approach which reduces the number of required experiments.

The preference of a modeling approach led to the application of receptance coupling [16] to predict the tool point FRF. In the initial application of receptance coupling to tool point FRF prediction, an Euler-Bernoulli (E-B) beam model of the overhung portion of the tool was coupled to the displacement-to-force receptance of the holder-spindle-machine [4]. The fluted portion of the tool was approximated using the equivalent diameter approach by Kops and Vo [5]. Many improvements have been made since then to the RCSA method. Park *et al.* incorporated displacement-to-moment, rotation-to-force and rotation-to-moment receptances in the analysis [17]. The E-B beam model was replaced with the Timoshenko beam model that takes into consideration the rotational inertia and shear deformation [18]. Schmitz *et al.* extended the RCSA method to three components: the overhung tool (i.e., the portion outside the holder), holder and spindle-machine [6]. The RCSA method was further improved by making use of FEA to estimate the stiffness and damping values at the tool-shrink fit holder connection [7]. FEA was implemented to model the spindle by Eturk *et al.* [19]. In the most recent study, Filiz *et al.* applied the spectral-Tchebychev technique to model the cutting tool [20].

CHAPTER 2
RECEPTANCE COUPLING SUBSTRUCTURE ANALYSIS

Description

This chapter describes the Receptance Coupling Substructure Analysis (RCSA) approach. In RCSA the receptances, or frequency response functions (FRFs), of individual components are coupled analytically to predict the assembly receptances. It involves both experimental and modeled FRFs. The tool-holder-spindle-machine assembly is divided into separate components. In the second generation RCSA method, the assembly was divided into three primary components: the tool, holder and spindle-machine [6]. The tool and holder were modeled, while the receptances of the spindle-machine (which are difficult to model based on first principles, primarily due to the difficulty in estimating damping at interfaces) were calculated by measuring a standard artifact and using the inverse receptance coupling method [6]. This approach is depicted in Figure 2-1. In Figure 2-2, four components are identified because the fluted portion of the tool is separated from the constant diameter tool shank.

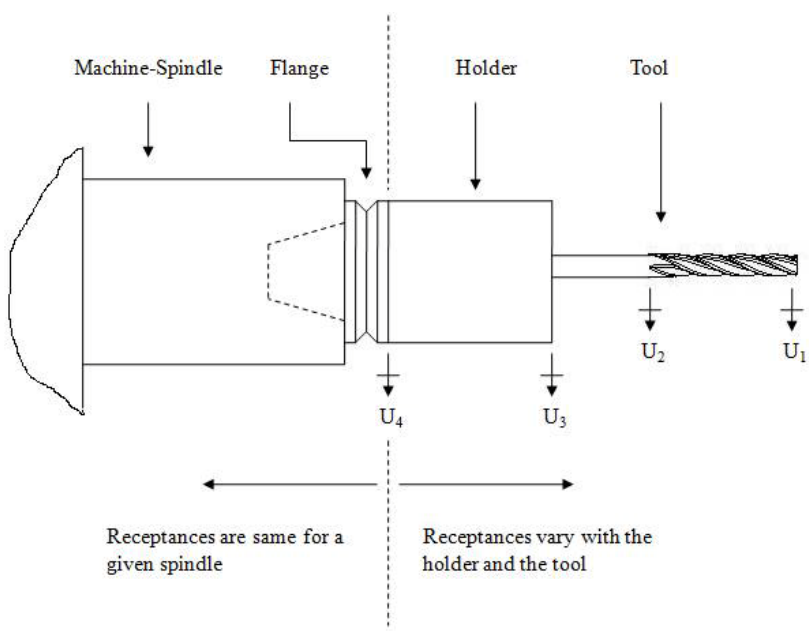

Figure 2-1. Tool-holder-spindle-machine assembly and coordinates

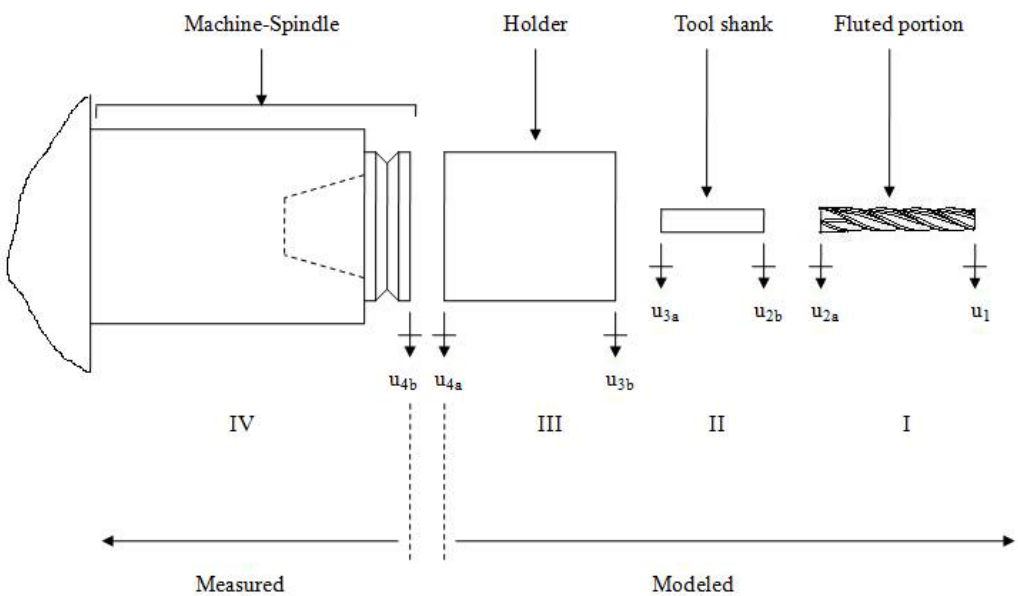

Figure 2-2. The machine assembly is divided into four components I- IV.

A FRF is a transfer function (expressed in frequency domain) where only the positive frequencies are considered. FRFs of a system are expressed as complex ratios of displacement-to-force, velocity-to-force or acceleration-to-force at the specified coordinate locations. They describe the system natural frequencies and mode shapes. The FRFs representing displacement–to-force are termed receptances. The complex ratio of the displacement to the applied force is either expressed as its real and imaginary parts or in terms of its magnitude and phase. The receptance of the tool-holder-spindle-machine assembly as reflected at the tool point is used to produce the desired stability lobe diagram.

For the tool-holder-spindle-machine RCSA model, four bending receptances are considered for the description of each component. They are,

displacement-to-force, $h_{ij} = \dfrac{x_i}{f_j}$

displacement-to-couple, $l_{ij} = \dfrac{x_i}{m_j}$

rotation-to-force, $n_{ij} = \frac{\theta_i}{f_j}$ and

rotation-to-couple, $p_{ij} = \frac{\theta_i}{m_j}$, where *i* and *j* are the coordinate locations.

If *i* and *j* are equal, the receptances are referred to as direct receptances; otherwise, they are denoted cross receptances. The receptances can either be measured or predicted. Due to the generally large number of tool, holder and spindle combinations in a particular facility, measuring FRFs can be very time consuming. Thus, to save time and improve efficiency, the receptances of the assembly components may be modeled using Euler-Bernoulli [16] or Timoshenko beam theory [21].

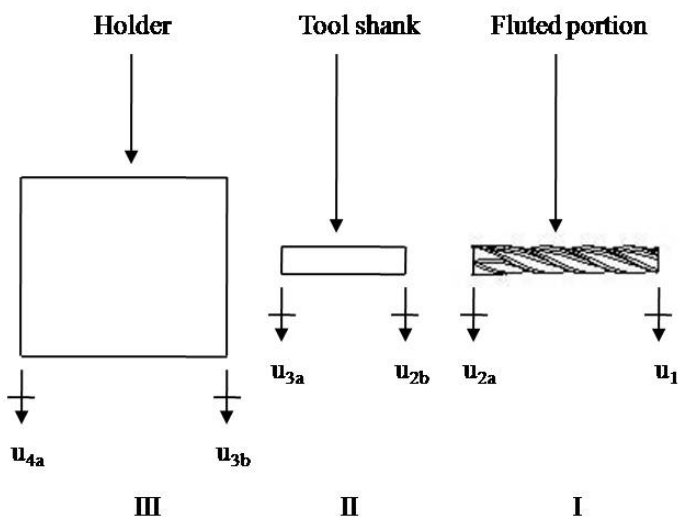

Figure 2-3. Components of the modeled sub-assembly: fluted portion (I), tool shank (II) and holder (III).

Free-Free Beam Receptances

Because the spindle-machine receptances are difficult to model, they are measured using a standard holder, while the tool and holder receptances are modeled. In this research the numerical (finite) Timoshenko beam elements are used to model the four degrees of freedom (displacement and rotations at both the ends) for free-free beam receptances of the tool shank

and holder [6]. Both FEA and equivalent diameter Timoshenko beam models are used to describe the fluted portion of the tool. See Figure 2-3, where rigid connections are assumed.

The individual component, or substructure, receptances, $R_{ij}(\omega)$, are defined in Equation 2-1:

$$R_{ij} = \begin{bmatrix} \frac{x_i}{f_j} & \frac{x_i}{m_j} \\ \frac{\theta_i}{f_j} & \frac{\theta_i}{m_j} \end{bmatrix} = \begin{bmatrix} h_{ij} & l_{ij} \\ n_{ij} & p_{ij} \end{bmatrix}, \tag{2-1}$$

where x_i is the substructure displacement at the coordinate location *i*, θ_i is the substructure rotation at the coordinate location *i*, f_j is the force applied to the substructure at the coordinate location *j* and m_j is the couple applied to the substructure at the coordinate location *j*.

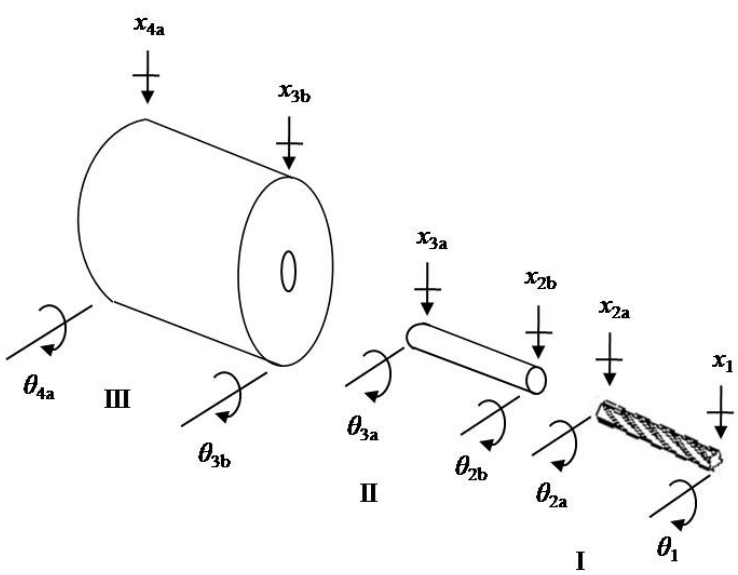

Figure 2-4. Individual components I-II-III with displacements and rotations at specified coordinate locations.

Thus, for the components I, II and III, Equations 2-2 to 2-13 describe the direct and cross receptances at the coordinate locations shown in Figure 2-4. Component I, the fluted portion of the tool, is described using Equations 2-2 through 2-5.

$$R_{11} = \begin{bmatrix} \frac{x_1}{f_1} & \frac{x_1}{m_1} \\ \frac{\theta_1}{f_1} & \frac{\theta_1}{m_1} \end{bmatrix} = \begin{bmatrix} h_{11} & l_{11} \\ n_{11} & p_{11} \end{bmatrix} \tag{2-2}$$

$$R_{12a} = \begin{bmatrix} \frac{x_1}{f_{2a}} & \frac{x_1}{m_{2a}} \\ \frac{\theta_1}{f_{2a}} & \frac{\theta_1}{m_{2a}} \end{bmatrix} = \begin{bmatrix} h_{12a} & l_{12a} \\ n_{12a} & p_{12a} \end{bmatrix} \tag{2-3}$$

$$R_{2a2a} = \begin{bmatrix} \frac{x_{2a}}{f_{2a}} & \frac{x_{2a}}{m_{2a}} \\ \frac{\theta_{2a}}{f_{2a}} & \frac{\theta_{2a}}{m_{2a}} \end{bmatrix} = \begin{bmatrix} h_{2a2a} & l_{2a2a} \\ n_{2a2a} & p_{2a2a} \end{bmatrix} \tag{2-4}$$

$$R_{2a1} = \begin{bmatrix} \frac{x_{2a}}{f_1} & \frac{x_{2a}}{m_1} \\ \frac{\theta_{2a}}{f_1} & \frac{\theta_{2a}}{m_1} \end{bmatrix} = \begin{bmatrix} h_{2a1} & l_{2a1} \\ n_{2a1} & p_{2a1} \end{bmatrix} \tag{2-5}$$

Similarly, component II, the tool shank, is described by Equations 2-6 through 2-9.

$$R_{2b2b} = \begin{bmatrix} \frac{x_{2b}}{f_{2b}} & \frac{x_{2b}}{m_{2b}} \\ \frac{\theta_{2b}}{f_{2b}} & \frac{\theta_{2b}}{m_{2b}} \end{bmatrix} = \begin{bmatrix} h_{2b2b} & l_{2b2b} \\ n_{2b2b} & p_{2b2b} \end{bmatrix} \tag{2-6}$$

$$R_{2b3a} = \begin{bmatrix} \frac{x_{2b}}{f_{3a}} & \frac{x_{2b}}{m_{3a}} \\ \frac{\theta_{2b}}{f_{3a}} & \frac{\theta_{2b}}{m_{3a}} \end{bmatrix} = \begin{bmatrix} h_{2b3a} & l_{2b3a} \\ n_{2b3a} & p_{2b3a} \end{bmatrix} \tag{2-7}$$

$$R_{3a3a} = \begin{bmatrix} \frac{x_{3a}}{f_{3a}} & \frac{x_{3a}}{m_{3a}} \\ \frac{\theta_{3a}}{f_{3a}} & \frac{\theta_{3a}}{m_{3a}} \end{bmatrix} = \begin{bmatrix} h_{3a3a} & l_{3a3a} \\ n_{3a3a} & p_{3a3a} \end{bmatrix} \tag{2-8}$$

$$R_{3a2b} = \begin{bmatrix} \dfrac{x_{3a}}{f_{2b}} & \dfrac{x_{3a}}{m_{2b}} \\ \dfrac{\theta_{3a}}{f_{2b}} & \dfrac{\theta_{3a}}{m_{2b}} \end{bmatrix} = \begin{bmatrix} h_{3a2b} & l_{3a2b} \\ n_{3a2b} & p_{3a2b} \end{bmatrix} \tag{2-9}$$

The component III, holder, receptances are given by Equations 2-10 through 2-13.

$$R_{3b3b} = \begin{bmatrix} \dfrac{x_{3b}}{f_{3b}} & \dfrac{x_{3b}}{m_{3b}} \\ \dfrac{\theta_{3b}}{f_{3b}} & \dfrac{\theta_{3b}}{m_{3b}} \end{bmatrix} = \begin{bmatrix} h_{3b3b} & l_{3b3b} \\ n_{3b3b} & p_{3b3b} \end{bmatrix} \tag{2-10}$$

$$R_{3b4a} = \begin{bmatrix} \dfrac{x_{3b}}{f_{4a}} & \dfrac{x_{3b}}{m_{4a}} \\ \dfrac{\theta_{3b}}{f_{4a}} & \dfrac{\theta_{3b}}{m_{4a}} \end{bmatrix} = \begin{bmatrix} h_{3b4a} & l_{3b4a} \\ n_{3b4a} & p_{3b4a} \end{bmatrix} \tag{2-11}$$

$$R_{4a4a} = \begin{bmatrix} \dfrac{x_{4a}}{f_{4a}} & \dfrac{x_{4a}}{m_{4a}} \\ \dfrac{\theta_{4a}}{f_{4a}} & \dfrac{\theta_{4a}}{m_{4a}} \end{bmatrix} = \begin{bmatrix} h_{4a4a} & l_{4a4a} \\ n_{4a4a} & p_{4a4a} \end{bmatrix} \tag{2-12}$$

$$R_{4a3b} = \begin{bmatrix} \dfrac{x_{4a}}{f_{3b}} & \dfrac{x_{4a}}{m_{3b}} \\ \dfrac{\theta_{4a}}{f_{3b}} & \dfrac{\theta_{4a}}{m_{3b}} \end{bmatrix} = \begin{bmatrix} h_{4a3b} & l_{4a3b} \\ n_{4a3b} & p_{4a3b} \end{bmatrix} \tag{2-13}$$

The relationships between displacements/rotations and forces/couples can be written in matrix form for convenience as shown in Equations 2-14 to 2-25.

$$\begin{Bmatrix} x_1 \\ \theta_1 \end{Bmatrix} = \begin{bmatrix} h_{11} & l_{11} \\ n_{11} & p_{11} \end{bmatrix} \begin{Bmatrix} f_1 \\ m_1 \end{Bmatrix} \text{ or } \{u_1\} = [R_{11}]\{q_1\} \tag{2-14}$$

Similarly,

$$\{u_1\} = [R_{12a}]\{q_{2a}\} \tag{2-15}$$

$$\{u_{2a}\} = [R_{2a2a}]\{q_{2a}\} \tag{2-16}$$

$$\{u_{2a}\} = [R_{2a1}]\{q_1\} \tag{2-17}$$

$$\{u_{2b}\} = [R_{2b2b}]\{q_{2b}\} \tag{2-18}$$

$$\{u_{2b}\} = [R_{2b3a}]\{q_{3a}\} \tag{2-19}$$

$$\{u_{3a}\} = [R_{3a3a}]\{q_{3a}\} \tag{2-20}$$

$$\{u_{3a}\} = [R_{3a2b}]\{q_{2b}\} \tag{2-21}$$

$$\{u_{3b}\} = [R_{3b3b}]\{q_{3b}\} \tag{2-22}$$

$$\{u_{3b}\} = [R_{3b4a}]\{q_{4a}\} \tag{2-23}$$

$$\{u_{4a}\} = [R_{4a4a}]\{q_{4a}\} \tag{2-24}$$

$$\{u_{4a}\} = [R_{4a3b}]\{q_{3b}\}, \tag{2-25}$$

where u_i and q_i are the generalized displacement/rotation and the force/couple vectors, respectively.

Coupling Free-Free Receptances

The coupling of the individual component receptances is performed sequentially with components I and II coupled first. Then, this subassembly's receptances are coupled with component III. The component I and II subassembly receptances are determined using Equations 2-28 to 2-44. In order to calculate the subassembly receptances, G_{11} (direct) and G_{3a1} (cross) (Equations 2-26 and 2-27, respectively), a generalized force Q_1 (representing both the externally applied force and couple) is applied at coordinate location 1(see Figure 2-5).

$$G_{11} = \begin{bmatrix} \dfrac{X_1}{F_1} & \dfrac{X_1}{M_1} \\ \dfrac{\Theta_1}{F_1} & \dfrac{\Theta_1}{M_1} \end{bmatrix} = \begin{bmatrix} H_{11} & L_{11} \\ N_{11} & P_{11} \end{bmatrix} \tag{2-26}$$

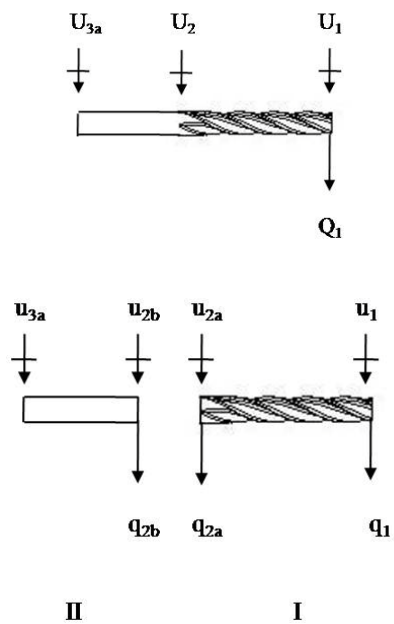

Figure 2-5. Subassembly composed of the fluted portion (I) and tool shank (II). The generalized force Q_1 is applied at U_1 to determine subassembly receptances G_{11}(direct) and G_{3a1}(cross).

$$G_{3a1} = \begin{bmatrix} \dfrac{X_{3a}}{F_1} & \dfrac{X_{3a}}{M_1} \\ \dfrac{\Theta_{3a}}{F_1} & \dfrac{\Theta_{3a}}{M_1} \end{bmatrix} = \begin{bmatrix} H_{3a1} & L_{3a1} \\ N_{3a1} & P_{3a1} \end{bmatrix} \tag{2-27}$$

The displacement equations for the substructures can be described as follows:

$$u_1 = R_{11}q_1 + R_{12a}q_{2a} \tag{2-28}$$

$$u_{2a} = R_{2a2a}q_{2a} + R_{2a1}q_1 \tag{2-29}$$

$$u_{2b} = R_{2b2b}q_{2b} \tag{2-30}$$

$$u_{3a} = R_{3a2b}q_{2b}\,. \tag{2-31}$$

If rigid coupling between the two components is assumed, the compatibility condition is expressed as shown in Equation 2-32.

$$u_{2b} - u_{2a} = 0 \tag{2-32}$$

The equilibrium condition at coordinate locations 2*a* and 2*b* is given by Equation 2-33.

$$q_{2b} + q_{2a} = 0 \tag{2-33}$$

At coordinate location 1, the equilibrium condition is provided by Equation 2-34.

$$q_1 = Q_1 \tag{2-34}$$

Substituting for u_{2b} and u_{2a} in Equation 2-32 gives Equation 2-35.

$$u_{2b} - u_{2a} = R_{2b2b}q_{2b} - R_{2a2a}q_{2a} - R_{2a1}q_1 = 0 \tag{2-35}$$

Equation 2-36 is obtained using Equations 2-33 and 2-34.

$$(R_{2b2b} + R_{2a2a})q_{2b} - R_{2a1}Q_1 = 0 \tag{2-36}$$

Solving for q_{2b} gives Equation 2-37. Given that $q_{2a} = -q_{2b}$ from Equation 2-33, substitution in Equation 2-38 gives Equation 2-39, which can then be written as shown in Equation 2-40.

$$q_{2b} = (R_{2b2b} + R_{2a2a})^{-1} R_{2a1}Q_1 \tag{2-37}$$

$$G_{11} = \frac{U_1}{Q_1} = \frac{u_1}{Q_1} = \frac{R_{11}q_1 + R_{12a}q_{2a}}{Q_1} \tag{2-38}$$

$$G_{11} = \frac{R_{11}Q_1 - R_{12a}(R_{2b2b} + R_{2a2a})^{-1} R_{2a1}Q_1}{Q_1} \tag{2-39}$$

$$G_{11} = R_{11} - R_{12a}(R_{2b2b} + R_{2a2a})^{-1} R_{2a1} = \begin{bmatrix} H_{11} & L_{11} \\ N_{11} & P_{11} \end{bmatrix} \tag{2-40}$$

Similarly, the cross receptances between coordinates 3*a* and 1 are given by Equations 2-41 and 2-42.

$$G_{3a1} = \frac{U_{3a}}{Q_1} = \frac{u_{3a}}{Q_1} = \frac{R_{3a2b}q_{2b}}{Q_1} = \frac{R_{3a2b}(R_{2b2b} + R_{2a2a})^{-1} R_{2a1}Q_1}{Q_1} \tag{2-41}$$

$$G_{3a1} = R_{3a2b}(R_{2b2b} + R_{2a2a})^{-1} R_{2a1} = \begin{bmatrix} H_{3a1} & L_{3a1} \\ N_{3a1} & P_{3a1} \end{bmatrix} \tag{2-42}$$

To determine the other two receptances of the sub-assembly I-II, G_{3a3a} and G_{13a}, a generalized force Q_{3a} is applied to U_{3a} as shown in Figure 2-6.

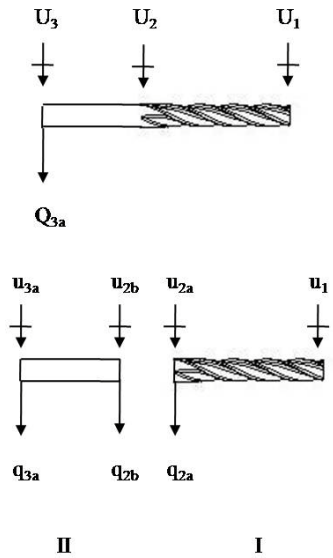

Figure 2-6. Subassembly composed of the fluted portion (I) and tool shank (II). The generalized force Q_{3a} is applied at U_{3a} to determine assembly receptances G_{3a3a} (direct) and G_{13a} (cross).

$$G_{3a3a} = \begin{bmatrix} \dfrac{X_{3a}}{F_{3a}} & \dfrac{X_{3a}}{M_{3a}} \\ \dfrac{\Theta_{3a}}{F_{3a}} & \dfrac{\Theta_{3a}}{M_{3a}} \end{bmatrix} = \begin{bmatrix} H_{3a3a} & L_{3a} \\ N_{3a3a} & P_{3a} \end{bmatrix} \tag{2-43}$$

$$G_{13a} = \begin{bmatrix} \dfrac{X_1}{F_{3a}} & \dfrac{X_1}{M_{3a}} \\ \dfrac{\Theta_1}{F_{3a}} & \dfrac{\Theta_1}{M_{3a}} \end{bmatrix} = \begin{bmatrix} H_{13a} & L_{13a} \\ N_{13a} & P_{13a} \end{bmatrix} \tag{2-44}$$

The component displacement/rotation equations are now described by Equations 2-45 to 2-48.

$$u_1 = R_{12a} q_{2a} \tag{2-45}$$

$$u_{2a} = R_{2a2a} q_{2a} \tag{2-46}$$

$$u_{2b} = R_{2b2b} q_{2b} + R_{2b3a} q_{3a} \tag{2-47}$$

$$u_{3a} = R_{3a3a} q_{3a} + R_{3a2b} q_{2b} \tag{2-48}$$

The compatibility equation remains the same as given in Equation 2-32.

$$u_{2a} - u_{2b} = 0 \tag{2-49}$$

The equilibrium equations are:

$$q_{2b} + q_{2a} = 0 \text{ and} \tag{2-50}$$

$$q_{3a} = Q_{3a} \,. \tag{2-51}$$

Substituting for u_{2a} and u_{2b} in Equation 2-49 gives Equation 2-52.

$$u_{2a} - u_{2b} = R_{2a2a} q_{2a} - R_{2b2b} q_{2b} - R_{2b3a} q_{3a} = 0 \tag{2-52}$$

Using Equations 2-50 and 2-51 and substituting for q_{2b} and q_{3a} in Equation 2-52 gives Equation 2-53.

$$(R_{2b2b} + R_{2a2a}) q_{2a} - R_{2b3a} Q_{3a} = 0 \tag{2-53}$$

Solving for q_{2a}, Equation 2-54 is obtained. Using Equation 2-20, q_{2b} can be written. Equation 2-55 gives the desired expression for the subassembly direct receptances.

$$q_{2a} = (R_{2b2b} + R_{2a2a})^{-1} R_{2b3a} Q_{3a} \tag{2-54}$$

$$G_{3a3a} = \frac{U_{3a}}{Q_{3a}} = \frac{u_{3a}}{Q_{3a}} = \frac{R_{3a3a} q_{3a} + R_{3a2b} q_{2b}}{Q_{3a}} \tag{2-55}$$

By substituting for q_{2b} in Equation 2-55 and using Equations 2-50 and 2-54, Equation 2-56 is obtained. Equation 2-57 gives the final expression after simplification.

$$G_{3a3a} = \frac{R_{3a3a} Q_{3a} - R_{3a2b} (R_{2b2b} + R_{2a2a})^{-1} R_{2b3a} Q_{3a}}{Q_{3a}} \tag{2-56}$$

$$G_{3a3a} = R_{3a3a} - R_{3a2b} (R_{2b2b} + R_{2a2a})^{-1} R_{2b3a} = \begin{bmatrix} H_{3a3a} & L_{3a3a} \\ N_{3a3a} & P_{3a3a} \end{bmatrix} \tag{2-57}$$

In a similar way, the cross receptances are defined. See Equations 2-58 and 2-59.

$$G_{13a} = \frac{U_1}{Q_{3a}} = \frac{u_1}{Q_{3a}} = \frac{R_{12a} q_{2a}}{Q_{3a}} = \frac{R_{12a}(R_{2b2b} + R_{2a2a})^{-1} R_{2b3a} Q_{3a}}{Q_{3a}} \tag{2-58}$$

$$G_{13a} = R_{12a}(R_{2b2b} + R_{2a2a})^{-1} R_{2b3a} = \begin{bmatrix} H_{13a} & L_{13a} \\ N_{13a} & P_{13a} \end{bmatrix} \tag{2-59}$$

The four receptances of the subassembly I-II are then rigidly coupled to the component III (holder) receptances. See Figure 2-7.

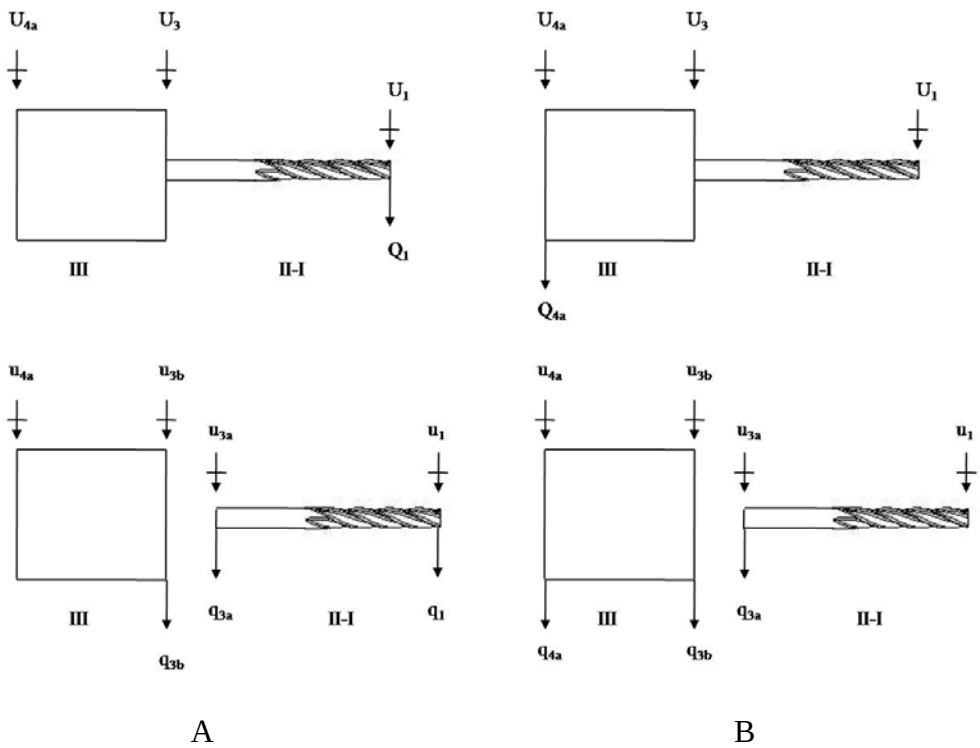

Figure 2-7. Component I-II (fluted portion and shank) subassembly receptances coupled with component III (holder) receptances.

The subassembly I-II and III direct and cross receptances are obtained in exactly the same manner as described for components I and II with the generalized force Q_1 applied at coordinate location 1 to determine the new G_{11} and G_{4a1} receptances (Figure 2-7A); Q_{4a} is applied at coordinate location 4*a* to determine G_{4a4a} and G_{14a} (Figure 2-7B). The resulting four receptances are described by Equations 2-60 to 2-64.

$$G_{11} = R_{11} - R_{13a}(R_{3b3b} + R_{3a3a})^{-1} R_{3a1} = \begin{bmatrix} H_{11} & L_{11} \\ N_{11} & P_{11} \end{bmatrix} \tag{2-60}$$

$$G_{4a1} = R_{4a3b}(R_{3b3b} + R_{3a3a})^{-1} R_{3a1} = \begin{bmatrix} H_{4a1} & L_{4a1} \\ N_{4a1} & P_{4a1} \end{bmatrix} \tag{2-61}$$

$$G_{4a4a} = R_{4a4a} - R_{4a3b}(R_{3b3b} + R_{3a3a})^{-1} R_{3b4a} = \begin{bmatrix} H_{4a4a} & L_{4a4a} \\ N_{4a3a} & P_{4a4a} \end{bmatrix} \tag{2-63}$$

$$G_{14a} = R_{13a}(R_{3b3b} + R_{3a3a})^{-1} R_{3b4a} = \begin{bmatrix} H_{14a} & L_{14a} \\ N_{14a} & P_{14a} \end{bmatrix} \tag{2-64}$$

Spindle-Machine Receptances

As discussed previously, the receptances of component IV (spindle–machine) are difficult to model. Therefore, these receptances are experimentally determined. Since the flange geometry is the same for all holders (to enable automatic tool changes), only the portion of the holder beyond the flange (towards the tool) is modeled. The flange and the holder taper (which is inserted in the spindle) are considered part of the spindle-machine. To identify the spindle-machine receptances, a standard artifact (i.e., a standard tool holder with a uniform cylindrical geometry beyond the flange) is placed in the spindle and G_{33} is measured as shown in Figure 2-8. Using G_{33} and a model of the portion of the holder beyond the flange, the spindle machine receptance R_{4b4b} is calculated. G_{33} is expressed in matrix form by replacing coordinate 1 by 3, 3*a* by 4*a* and 3*b* by 4*b* in Equation 2-60. See Equation 2-65.

$$G_{33} = R_{33} - R_{34a}(R_{4b4b} + R_{4a4a})^{-1} R_{4a3} = \begin{bmatrix} H_{33} & L_{33} \\ N_{33} & P_{33} \end{bmatrix} \tag{2-65}$$

If G_{33} is determined experimentally and R_{33}, R_{4a3}, R_{4a4a} and R_{34a} are modeled (component III in Figure 2-8), R_{4b4b} can be calculated by rewriting Equation 2-65 as shown in Equation 2-66. This is referred to as *inverse receptance coupling*.

$$R_{4b4b} = R_{4a3}\left(R_{33} - G_{33}\right)^{-1} R_{34a} - R_{4a4a} \tag{2-66}$$

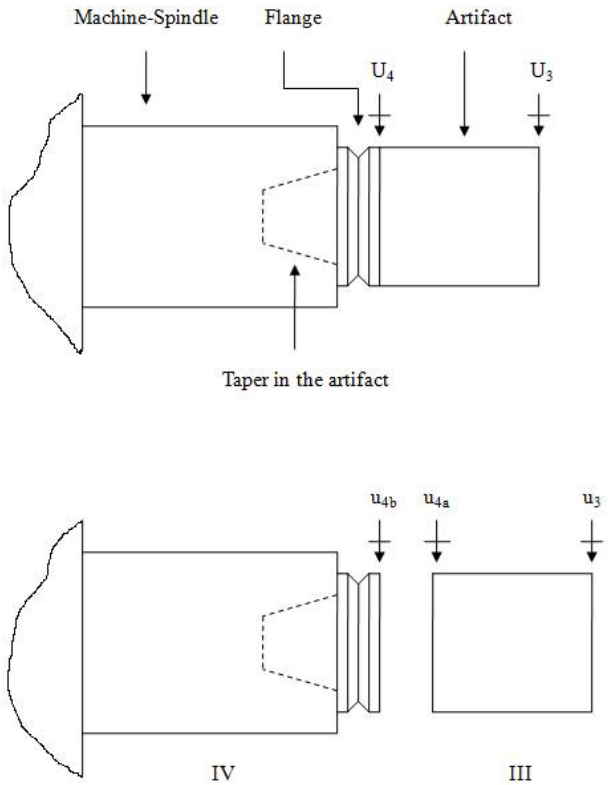

Figure 2-8. Standard artifact used to determine spindle-machine (component IV) receptances.

The component receptance H_{33} from the G_{33} matrix was measured by impact testing (the TXF software from MLI was used for data acquisition and signal analysis). In this method, an impact hammer is used to apply the force and an accelerometer (piezoelectric sensor) measures the accelerance (translational acceleration-to-force FRF) and the software is used to twice integrate the accelerance to give the required displacement-to-force receptance.

As shown in Figure 2-9, the direct FRF H_{33} is measured with the force and the accelerometer at the same coordinate location. A second component of the G_{33} matrix, N_{33}, is calculated by the finite difference approach [22] as described in Equation 2-67, where the cross

FRF H_{3a3} is measured as shown in Figure 2-10 and s is the distance between the direct and cross FRF measurements.

$$N_{33} = \frac{\theta_3}{f_3} = \frac{\frac{x_3 - x_{3a}}{s}}{f_3} = \frac{\frac{x_3}{f_3} - \frac{x_{3a}}{f_3}}{s} = \frac{H_3 - H_{33a3}}{s} \tag{2-67}$$

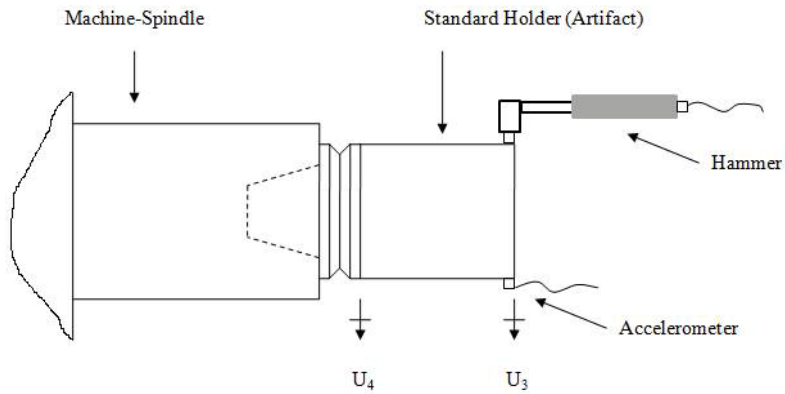

Figure 2-9. Measurement of H_{33} using impact testing.

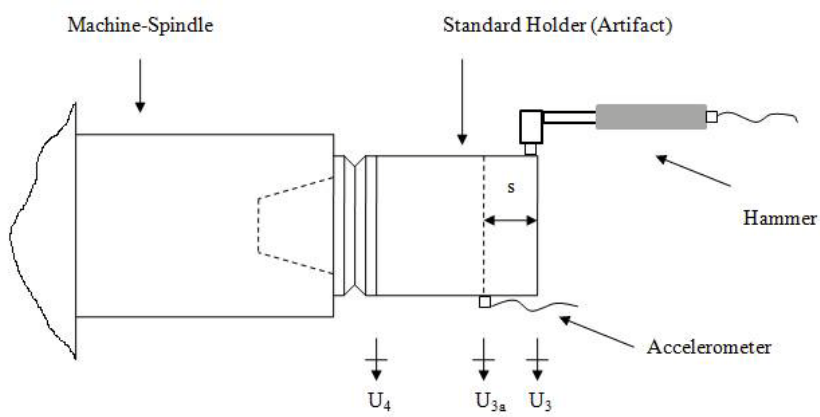

Figure 2-10. Measurement of H_{3a3} using to determine N_{33}.

Assuming reciprocity, the off-diagonal terms of the G_{33} matrix may be taken to be equal. See Equation 2-68.

$$L_{33} = N_{33} \tag{2-68}$$

The P_{33} receptance is synthesized using Equation 2-69 [22].

$$P_{33} = \frac{x_3}{m_3}\frac{\theta_3}{f_3}\frac{f_3}{x_3} = L_{33}N_{33}\frac{1}{H_{33}} = \frac{N_{33}{}^2}{H_{33}} \tag{2-69}$$

Thus, using inverse receptance coupling and the finite difference approach, the spindle-machine (component IV) receptances are obtained. These receptances can then be coupled with any fluted portion-tool shank-holder modeled receptances to predict the tool point assembly dynamics.

Collet Holder-Spindle-Machine Receptances

In this study, a collet holder was used and the holder-spindle-machine receptances were measured as a single subassembly. Therefore, the entire tool-holder-spindle-machine assembly was divided into only three components: the fluted portion of the tool (I), the tool shank (II) and the holder-spindle-machine (III). Components I and II were modeled as described previously. The measurements for component III included the direct FRF H_{33} and cross FRF H_{3a3}. The subassembly receptances L_{33}, N_{33} and P_{33} were determined as described in the previous section. Figures 2-11 through 2-14 show the measurements used to determine the components of matrix G_{33}.

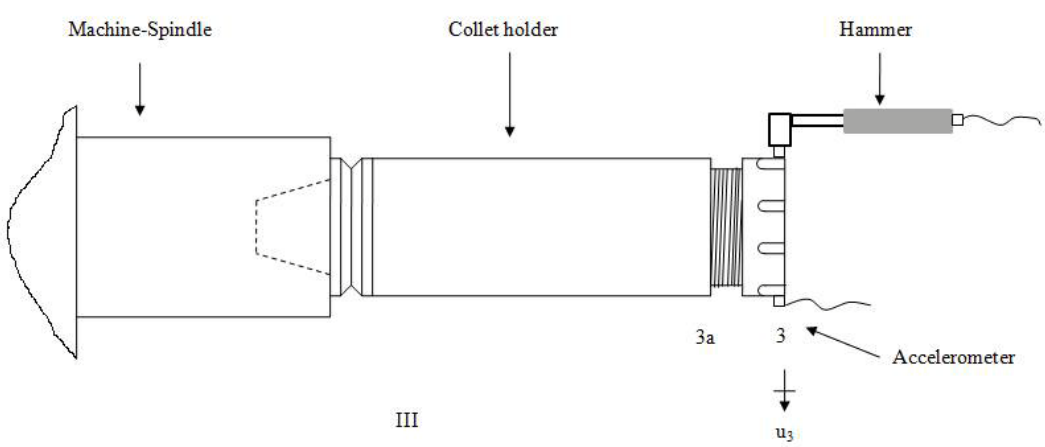

Figure 2-11. Measurement of component III (holder-spindle-machine) receptance, H_{33}.

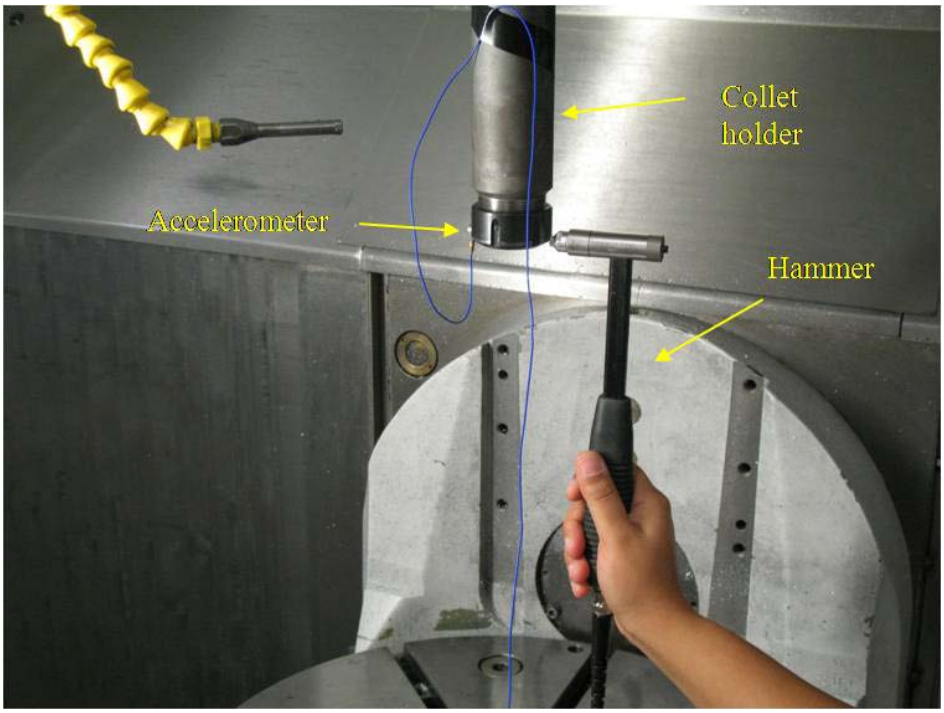

Figure 2-12. Impact testing to measure the direct receptance of the holder-spindle-machine assembly, H_{33}.

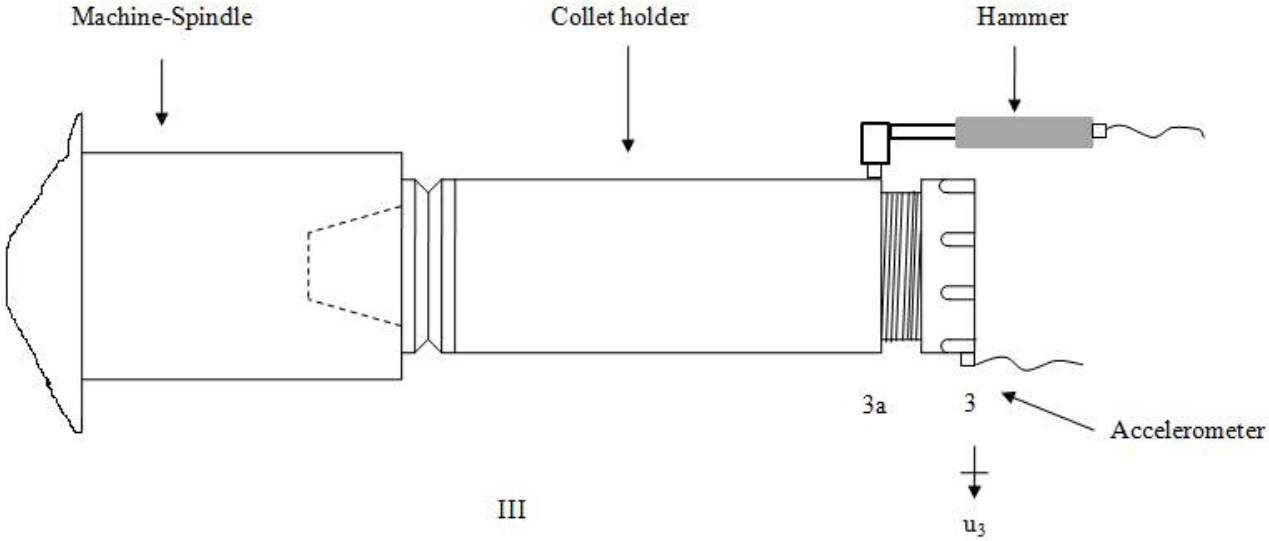

Figure 2-13. Measurement of component III (holder-spindle-machine) cross receptance, H_{33a} to determine N_{33}, L_{33} and P_{33}.

Figure 2-14. Impact testing to measure the cross receptance of the holder-spindle-machine assembly, H_{33a}.

H_{33} and H_{33a} were measured and N_{33}, L_{33} and P_{33} were calculated using Equations 2-67 through Equation 2-69, where s = 30 mm. The modeled tool receptances were then coupled to G_{33}. The predicted tool point frequency response was then compared to the measured tool point FRF. Figure 2-15 shows the experimental setup used to acquire the tool point FRF.

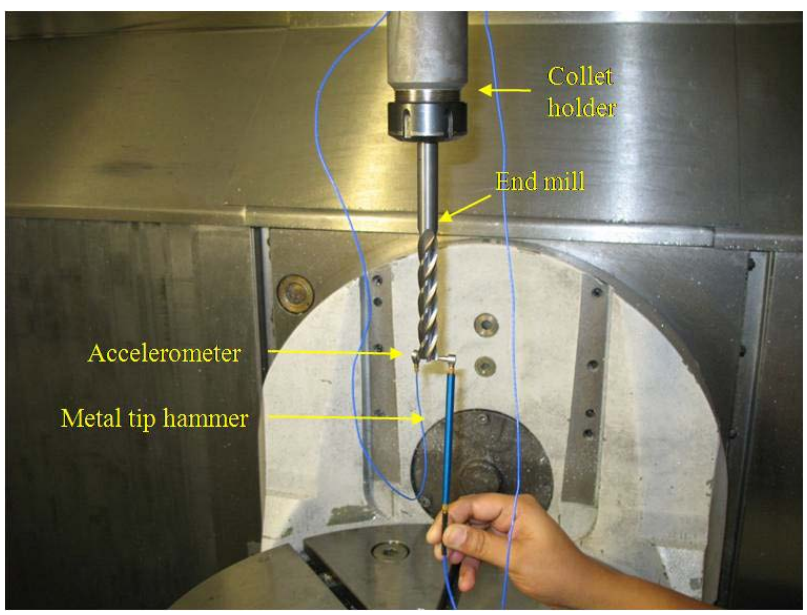

Figure 2-15. Impact testing to measure the tool point FRF of the tool-holder-spindle-machine assembly, H_{11}.

CHAPTER 3
MODELING AND ANALYSIS

End Mill Modeling

A three-dimensional (3D) model of the fluted portion of the four flute, carbide end mill shown in Figure 3-1 was developed in Pro-Engineer Wildfire (Pro-E).

Figure 3-1. Carbide end mill.

The model was then imported into ANSYS Workbench for the finite element analysis. The geometry of the end mill was: 12.7 mm shank diameter, 66.15 mm shank length, 85.05 mm fluted portion length, 30 deg helix angle, and 75 mm pitch. The steps used to model the geometry of the fluted portion in Pro-E are detailed next:

1. Using the command Extrude on the top plane, sketch a circle with diameter of the shank and then extrude it to the length of the fluted portion.

2. Select Insert>>Helical Sweep>>Cut.

3. Define the attributes, Constant>> Thru axis>> Right-handed>> Done

4. To specify the Sweep Profile, select the front plane. Draw a center axis at the center of the cylinder and, from the bottom left corner of the cylinder, draw a vertical line equal to the length of the cylinder, the arrow should be pointing upwards.

5. Specify the pitch value.

6. Define the section as shown in the Figure 3-2A. The section is drawn by measuring the dimensions as shown in Figure 3-2B. The horizontal line is the dimension on the face of the tool as indicated in the Figure 3-2B and the vertical line is the distance between two flutes in the front plane. The arc is tangent to the vertical and the two lines joining the arc to the vertical line represent the cutting edge. Specify the material side which should be inside the section.

7. Once the first flute is created, pattern it around the central axis to obtain four flutes.

8. Use the command Round to smooth the inner edge; the radius should be equal to the inner surface of the end mill as shown in Figure 3-3.

9. Save the part file as the .stp file type.

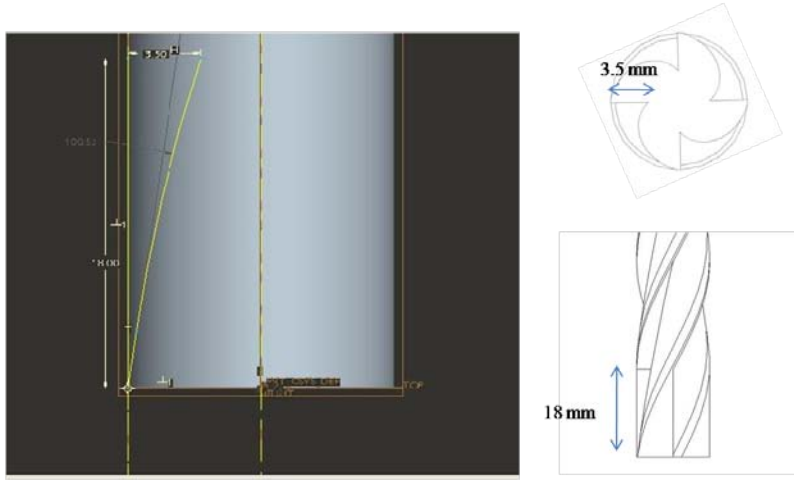

A B

Figure 3-2. A) Section drawn for helical sweep in Pro-E. B) Dimensions used to draw the section.

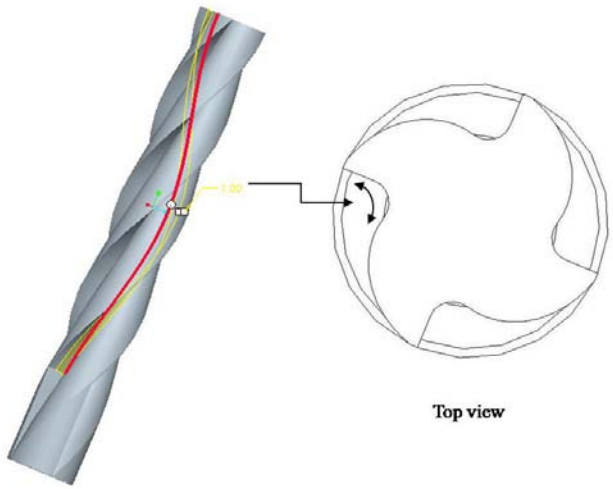

Figure 3-3. Rounding of the inner edge.

Figure 3-4. Final model of the fluted portion of end mill.

Analysis in ANSYS Workbench

The step file (.stp) created in Pro-E was then used to perform a harmonic analysis in ANSYS workbench to calculate the direct and cross receptances of the fluted portion of the end mill. The steps are next identified:

1. Open ANSYS Workbench. Select Empty Project>> New Geometry>> File>>Import External Geometry>> Generate.

2. Click on Project>> New Simulation

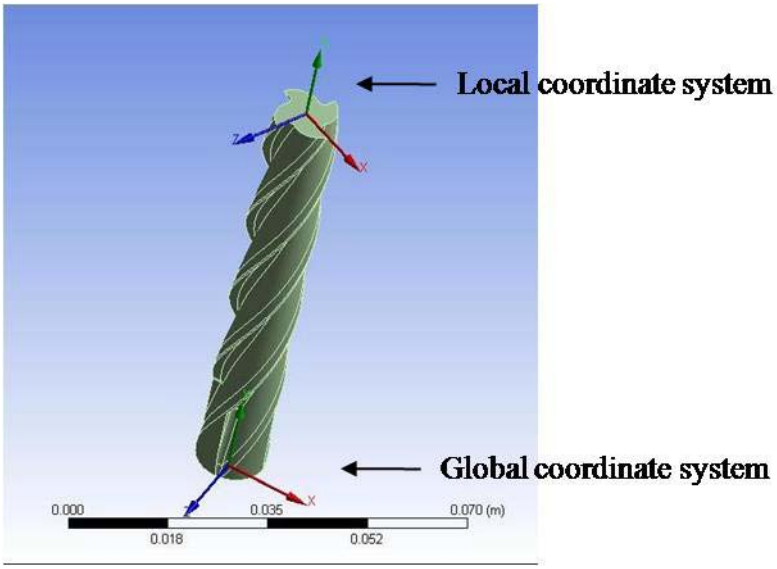

Figure 3-5. Local coordinate system defined on the end mill model.

3. Model>> Geometry>> Name of the geometry. The box on the bottom right side of the screen has an option for material type. Click on new material and specify the density, elastic (Young's) modulus and Poisson's ratio for the tool material (tungsten carbide in this case). The values used for this simulation are: 15000 kg/m^3 density, 5.5×10^{11} N/m^2 elastic modulus and 0.22 Poisson's ratio.

4. The coordinate system should be aligned such that the *x* axis is along the flute's cutting edge as shown in Figure 3-5.A local coordinate system is defined so that the *x* axis is along the edge of the flute.

5. For meshing, click on mesh option on the left side of the screen. Select the options for meshing. Size of the elements>> 5×10^{-4} m. This is the smallest size that can be chosen in Workbench. Right click on Mesh and click on generate mesh. The mesh generated in shown in Figure 3-6.

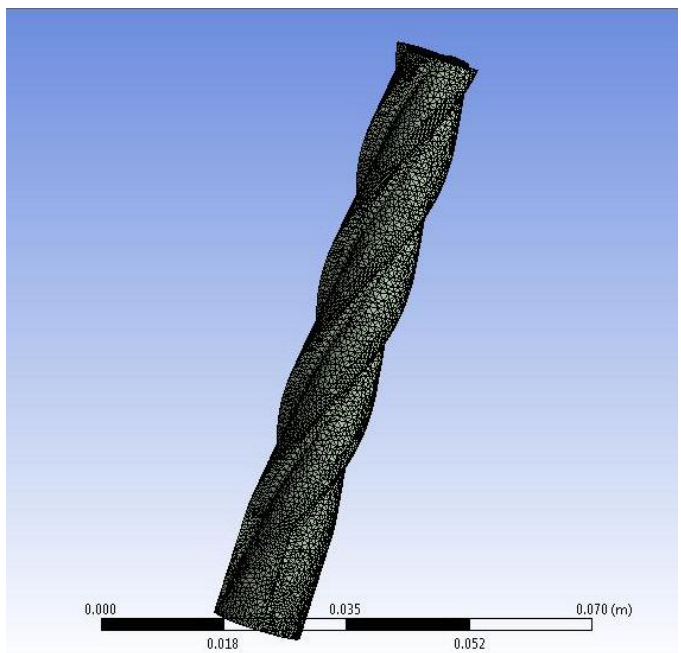

Figure 3-6. Meshing created on end mill model

6. In order to calculate the natural frequencies, a modal analysis was performed.

7. Insert New Analysis>> Modal Analysis>> Analysis Setting. Select the number of modes. Right click on Solution>>Insert>>Deformation>>Total. Click Solve.

8. The natural frequencies of the number of modes selected can then be viewed.

9. In order to calculate the receptances, a Harmonic Analysis was performed. The deformation of every node was stored in the .db file and read in ANSYS classic. New Analysis>> Harmonic Analysis>> Analysis settings. Insert the range of frequency and the

number of intervals. In this analysis, a resolution of 0.1 Hz was used. Select the Full method. Specify the damping constant (0.00075 in this case). Click Yes to save the .db file.

10. Right click on Analysis>> Insert>> Force/ Moment. Select the node where the force/moment needs to be applied. To specify the magnitude of force/moment select Components and also the coordinate system if you have specified any other than the Global Coordinates. In *x*/*y*/*z* component specify the force/moment (1 N along the *x* axis or 1 N-m about negative *z* axis in this case) shown in Figure 3-7 and Figure 3-8.

11. Right click on Solution and insert Frequency response>> Deformation. Select the vertex where the deformation is to be determined. In this case the vertex opposite to that where the force was applied was selected. Choose the Direction>> X Axis. Click on Solve.

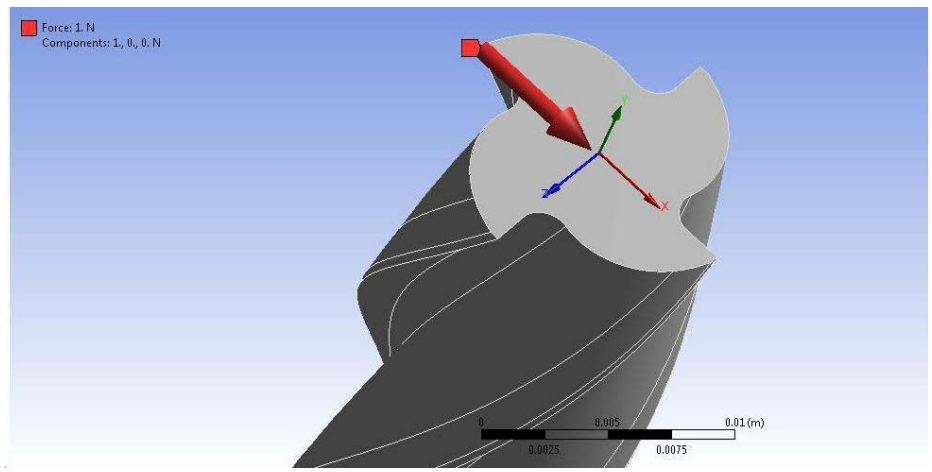

Figure 3-7. Force applied along the positive x axis.

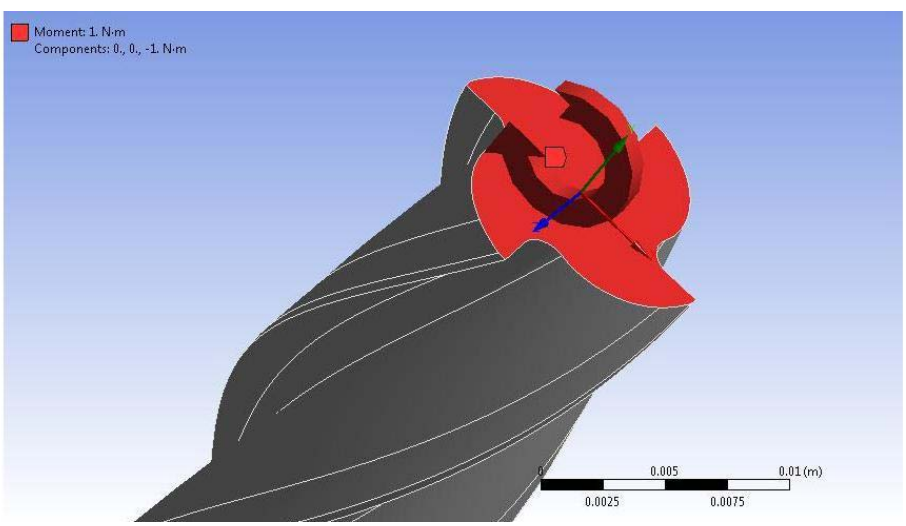

Figure 3-8. Moment applied on the top face about *z* axis.

Results from ANSYS Classic

The .db file saved from the harmonic analysis was imported into ANSYS Classic to read the results at particular nodes. The direct receptances, *h* and *l*, were calculated by finding the deformation in the *x* axis (which can be the global *x* axis or the *x* axis of the new coordinate system specified) on the node opposite to the node where force/moment was applied. To find the direct receptances, *n* and *p*, the deformations at nodes 1 and 2 shown in Figures 3-9 and 3-10 were read. The difference between the deformations divided by the distance between the nodes gave *l*. Similarly, for the cross-receptances, the nodes at the other end of the model were selected (see Figure 3-11).

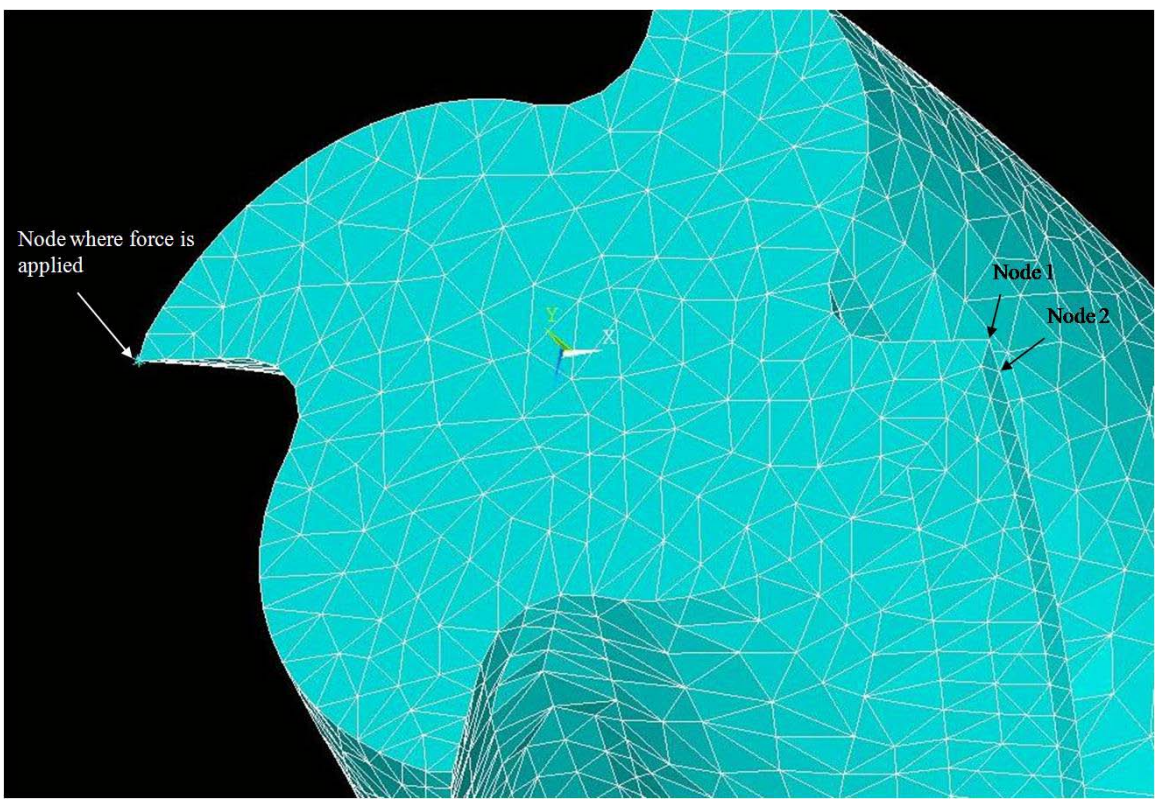

Figure 3-9. Nodes selected to obtain *h* and *l* receptances.

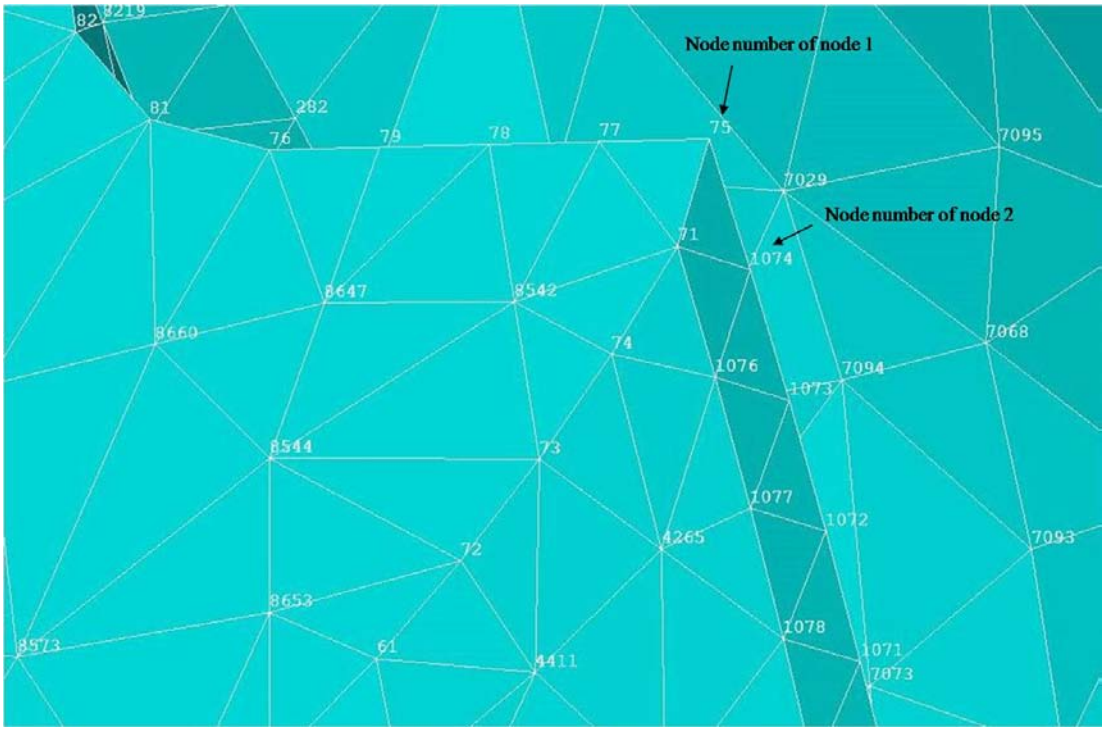

Figure 3-10. Numbers of selected nodes for direct receptances.

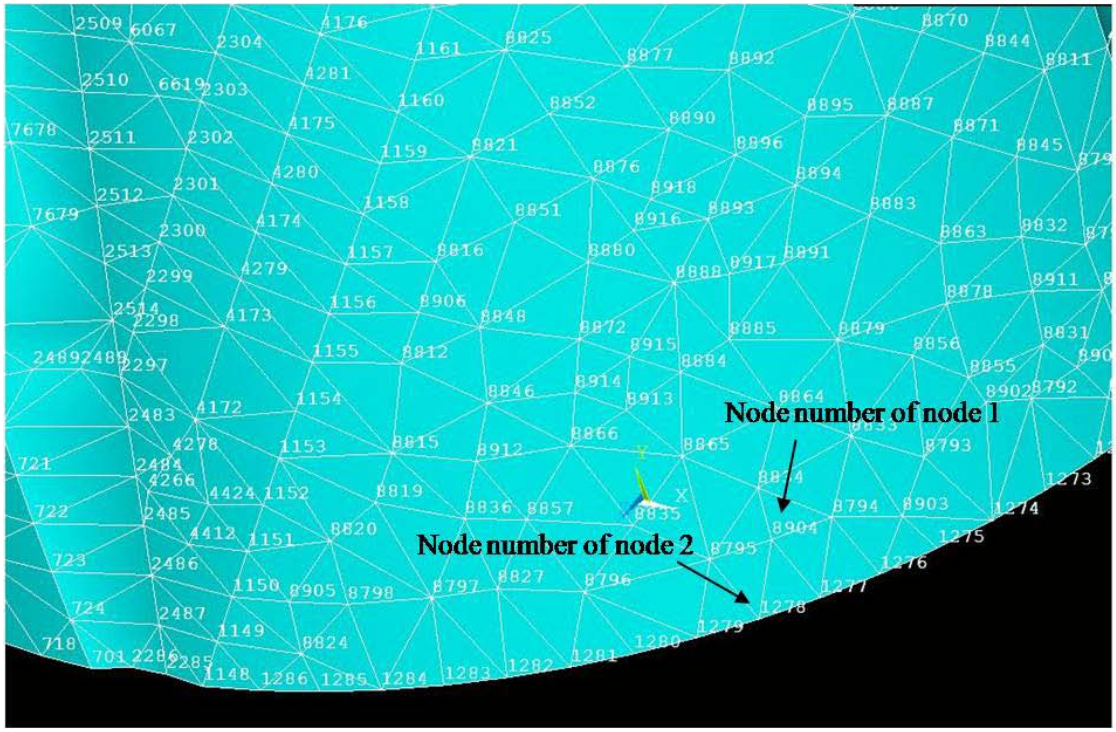

Figure 3-11. Numbers of selected nodes for cross receptances.

The steps followed in ANSYS Classic are next detailed:

1. Click on File>> Change Directory>> Select the folder where the .db file is stored.

2. File>> Resume from>> Click on the .db file.

3. In order to read the direct and cross *h* and *n* receptances and calculate the direct and cross *l* and *p* receptances, a program was written in APDL (ANSYS Parametric Design Language) provided in Appendix A. The result is stored in an .inp file. To read it, click on File>> read input from>>select the .inp file.

4. The real and imaginary values for all receptances are stored in an Excel file. This file can then be imported in MATLAB to plot the free-free receptances of the fluted portion and couple it with shank-holder-spindle-machine receptances to predict the tool point frequency response function.

CHAPTER 4
COMPARISON BETWEEN MODEL PREDICTIONS AND EXPERIMENTAL RESULTS

Free-Free Receptances of the End Mill

This section describes the three approaches used to obtain the free-free receptance ($h = x/f$) of the end mill. Each approach is described and the results are compared.

Experimental Approach

In the experimental approach, the frequency response function (FRF) of the end mill was obtained by impact testing. The free-free boundary conditions were approximated by placing the end mill on a piece of foam (Figure 4-1). The very low stiffness foam base (relative to the end mill) provided adequate conditions to obtain the free-free receptances of the end mill.

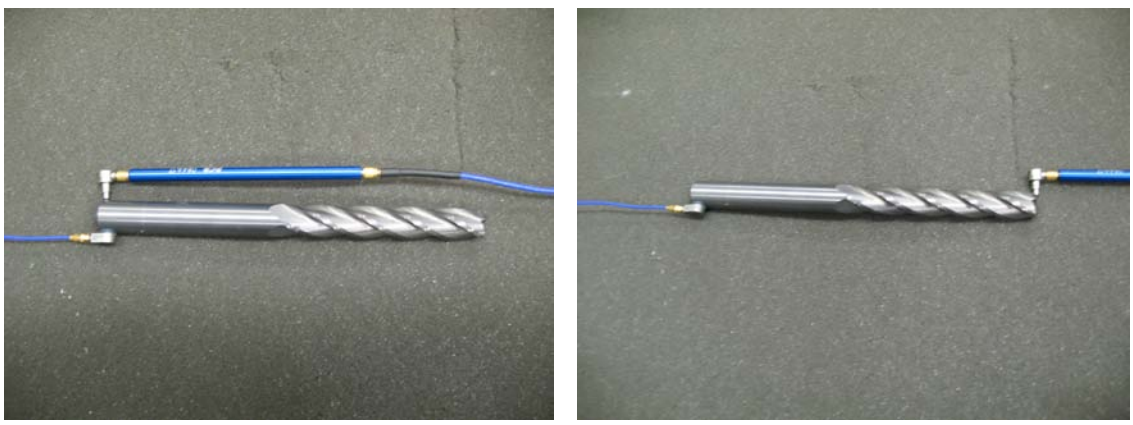

A B

Figure 4-1. Experimental free-free receptance by impact testing. A) Direct receptance. B) Cross receptance.

A low mass/metal tip (high contact stiffness) hammer was used to excite a wide range of frequencies simultaneously. The accelerometer mass was compensated to avoid the loading effects on the low mass tool. Using the mass cancellation approach [23] given by Equations 4-1 and 4-2, where $m_{accelerometer}$ is the accelerometer mass, the desired direct and cross accelerance FRFs were obtained. The direct and cross receptance FRFs were then defined by Equations 4-3 and 4-4, respectively.

$$A_{11,corrected} = \frac{A_{11,measured}}{1 - m_{accelerometer} A_{11,measured}} \tag{4-1}$$

$$A_{12,corrected} = \frac{A_{12,measured}}{1 - m_{accelerometer} A_{12,measured}} \tag{4-2}$$

$$H_{11} = \frac{A_{11,\text{corrected}}}{-\omega^2} \tag{4-3}$$

$$H_{12} = \frac{A_{12,\text{corrected}}}{-\omega^2} \tag{4-4}$$

Equivalent Diameter Approach

As mentioned previously, the equivalent diameter approach assumes a constant cross-section of the fluted portion of the end mill. The equivalent diameter of the cross section was calculated in three different ways.

1. The cross-sectional area of the fluted portion, A_f, was modeled and the corresponding equivalent diameter, d_{eqA}, was calculated. See Equation 4-5.

$$d_{eqA} = \sqrt{\frac{4A_f}{\pi}} \tag{4-5}$$

   Using the software Solidworks, the cross-sectional area of the modeled tool was determined [24]. The model considered in this work gave an area of 82.113 mm^2. Using Equation 4-5, the equivalent diameter was 7.23 mm.

2. The area moment of inertia for the modeled cross-section of the fluted portion, I_f, was determined using Solidworks and the equivalent diameter, d_{eqI}, was calculated using Equation 4-6

$$d_{eqI} = \sqrt[4]{\frac{64\, I_f}{\pi}} \tag{4-6}$$

   For the tested tool, the area moment of inertia was 595.25 mm^4, which gave an equivalent diameter of 10.494 mm.

3. The mass of the tool can be expressed as the sum of the mass of the shank (first expression on the left hand side of Equation 4-7) and the mass of the fluted portion (second expression):

$$\rho \frac{\pi d_s^2 L_s}{4} + \rho \frac{\pi d_{eqM}^2 L_f}{4} = m\,, \tag{4-7}$$

where m is total mass of the tool, d_s and d_{eqM} are the shank diameter and the equivalent diameter of the fluted portion, respectively, L_s and L_f are the lengths of the shank and the fluted portion, respectively, and ρ is the tool density (carbide for this study). By weighing the tool and substituting nominal value for the density and geometry of the tool, the equivalent diameter, d_{eqM}, was calculated according to Equation 4-8:

$$d_{eqM} = \sqrt{\frac{4}{\pi L_f}\left(\frac{m}{\rho} - \frac{\pi d_s^2 L_s}{4}\right)}\,, \tag{4-8}$$

where m = 216.5 g, L_s = 66.15 mm, L_f = 85.05, d_s = 12.7 mm and ρ = 0.015 g/mm^3. Using these values, an equivalent diameter of 9.525 mm was obtained. The mass of the fluted portion, m_f, can be expressed as shown in Equation 4-9.

$$\rho \frac{\pi d_{eqM}^2 L_f}{4} = m_f \tag{4-9}$$

Because the mass of the fluted portion m_f remains constant, the value of d_{eqM} also remains constant as it depends only on L_f and ρ, which do not change even if receptances are modeled at different overhang lengths, i.e., different values of L_s.

Finite Element Analysis (FEA) Approach

The free-free receptances of the fluted portion were obtained by harmonic analysis (using ANSYS Workbench as discussed in Chapter 3) and then rigidly coupled to the free-free receptances of the shank using RCSA. The free-free receptances for the shank were calculated using the Timoshenko beam model [6] programmed in MATLAB.

Comparison between the Three Approaches

The natural frequencies of the first bending mode for the fluted portion (only) of the end mill as determined by FEA and the three equivalent diameter approaches are compared in Table 4-1. Since it was not possible to measure the FRF of only the fluted portion, results from the experimental approach are not included.

Table 4-1. Comparison of first bending mode natural frequency (free-free boundary conditions) of the fluted portion of end mill obtained by FEA and equivalent diameter approaches.

Approach	Natural frequency (Hz)	Percentage error (relative to FEA)
FEA	6662	
d_{eqA}	5230	-21.5
d_{eqI}	7219	8.4
d_{eqM}	6804	2.1

Table 4-2 provides a comparison between the experimental, equivalent diameter and FEA approaches for free-free receptances of the entire end mill (tool shank coupled to the fluted portion).

Table 4-2. Comparison of the entire end mill (shank and fluted portion) free-free first bending mode natural frequency obtained using the three different approaches.

Approach	Natural frequency (Hz)	Percentage error (relative to experiment)
Experimental	2496	
FEA	2515	0.7
d_{eqA}	1641	-34.3
d_{eqI}	2493	-0.1
d_{eqM}	2217	-11.2

Using the FEA approach, the free-free receptances were obtained up to a frequency of 600 Hz for the fluted portion of the end mill. The time to compute the displacement-to-force receptance for a frequency range of 20 Hz with a resolution of 0.1 Hz was 20 hours, so the frequency range was limited to 600 Hz and the receptances at both the ends of the fluted portion were assumed to be the same. The significant computational expense of the FEA approach leads to the preference for an alternative, less costly approach. The first bending mode natural frequency obtained by coupling the fluted portion harmonic analysis receptances to the clamped-free Timoshenko beam model was compared to the natural frequency obtained by modal analysis in FEA for the clamped-free end mill (shown in Table 4-3). A long shank length was considered

so that the natural frequency was less than 600Hz. The difference between the two results was caused by the assumption of equal receptances on both the ends of fluted portion.

Table 4-3. Comparison of first bending mode natural frequency between clamped-free FEA modal analysis and coupling the harmonic analysis fluted portion receptances with a clamped-free Timoshenko shank model.

Shank length (mm)	Natural frequency (Hz)		
	FEA modal analysis (clamped-free)	Fluted portion receptances (harmonic analysis) coupled to Timoshenko beam model and rigid support	Percentage error
80	467	404	13.4
90	416	367	11.8
100	372	333	10.3

Due to the significant computational expense associated with the harmonic analysis, only the natural frequencies obtained by FEA modal analysis (computational time was approximately two to three minutes) were compared to the other approaches. The first bending natural frequency obtained by modal analysis was compared to the first bending natural frequency obtained by the equivalent diameter approach (which takes just over one minute to complete) to compare the three equivalent diameter calculation methods. Using the three equivalent diameters and the Timoshenko beam model, the clamped-free receptances were calculated by coupling the tool substructure (receptances of the fluted portion modeled using equivalent diameters coupled to the various shank lengths) to a rigid support (having zero receptances). Experiments were also performed by clamping the tool in a vise to approximate fixed-free boundary conditions (see Figure 4-2). Table 4-4 shows a comparison of the first clamped-free bending natural frequency obtained by FEA modal analysis, the equivalent diameter methods and experiment for different overhang lengths. Figure 4-3 shows the percentage error relative to experimental result versus the tool shank length for the three equivalent diameters and the FEA modal analysis results.

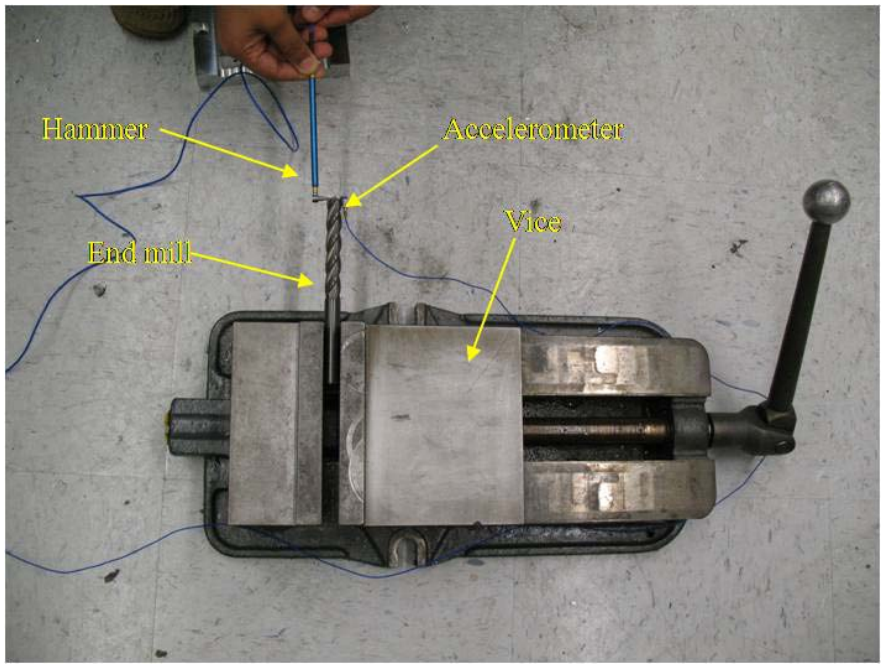

Figure 4-2. Experimental setup to measure clamped-free FRF of the end mill.

Table 4-4. Comparison of clamped-free first bending mode natural frequency between experiment, equivalent diameters and FEA modal analysis.

Overhang length (mm)	Natural frequency (Hz)					Percentage error relative to experiment			
	Exp	d_{eqA}	d_{eqM}	d_{eqI}	FEA	d_{eqA}	d_{eqM}	d_{eqI}	FEA
91.5	914	821	1047	1128	1234	-10.1	14.6	23.5	35.1
96.5	848	809	1004	1064	1156	-4.6	18.4	25.5	36.4
101.5	877	795	960	1001	1082	-9.3	9.4	14.2	23.3
106.5	867	781	916	941	1011	-10.0	5.6	8.5	16.5
111.5	833	765	872	884	944	-8.2	4.7	6.1	13.3
116.5	756	748	828	830	881	-1.0	9.6	9.8	16.6
121.5	712	730	786	779	823	2.6	10.5	9.4	15.6
126.5	671	711	746	731	769	6.1	11.2	9.0	14.7
131.5	629	692	706	686	719	10.0	12.3	9.1	14.3
136.5	568	671	668	644	673	18.2	17.6	13.4	18.4

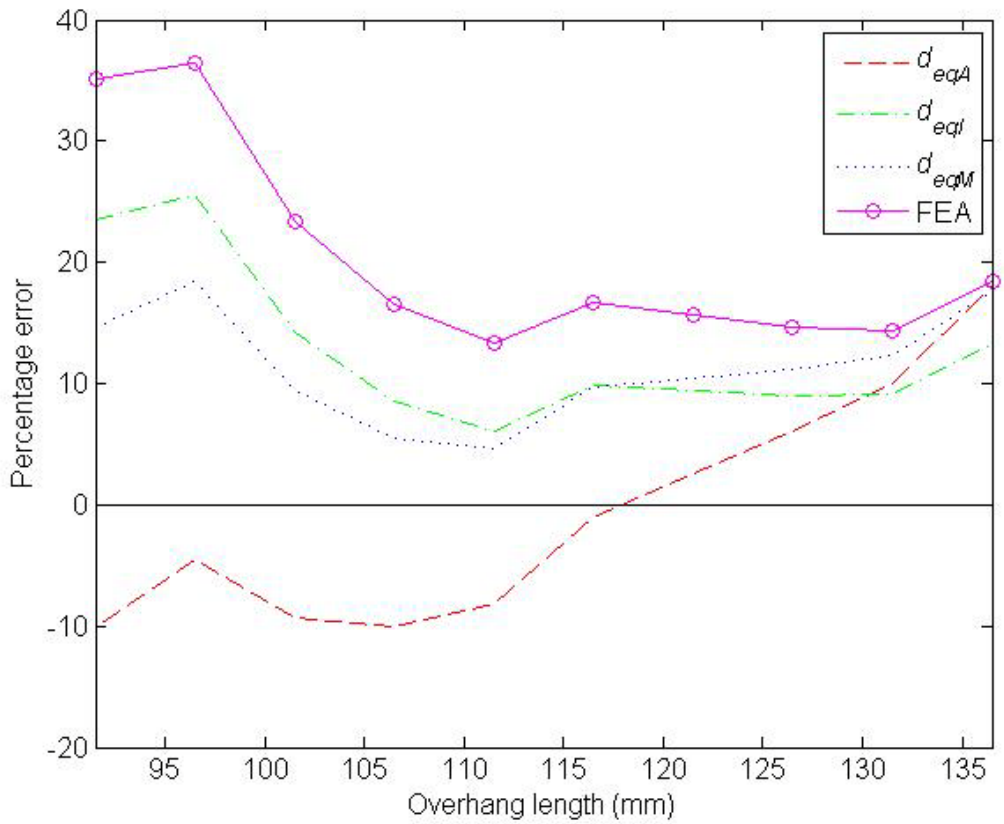

Figure 4-3. Percentage error (relative to experiment) for different equivalent diameters and FEA as a function of overhang length.

Figure 4-3 shows that the first bending mode natural frequency obtained by FEA has an error of 35% relative to the experimental validation for the shortest overhang length tested. It is proposed that the large error between the two approaches is due to imperfect realization of the clamped boundary condition (between the tool and vise). If this clamping condition is not exactly rigid, this effectively incorporates a linear/torsional “spring” at the vise-tool interface and would serve to lower the measured natural frequency(s). Assuming the FEA modal analysis provides the most accurate representation of the clamped-free tool, the FEA and equivalent diameter approaches were compared to experiment by normalizing the mean error between the experimental and FEA results to zero (see Figure 4-4).

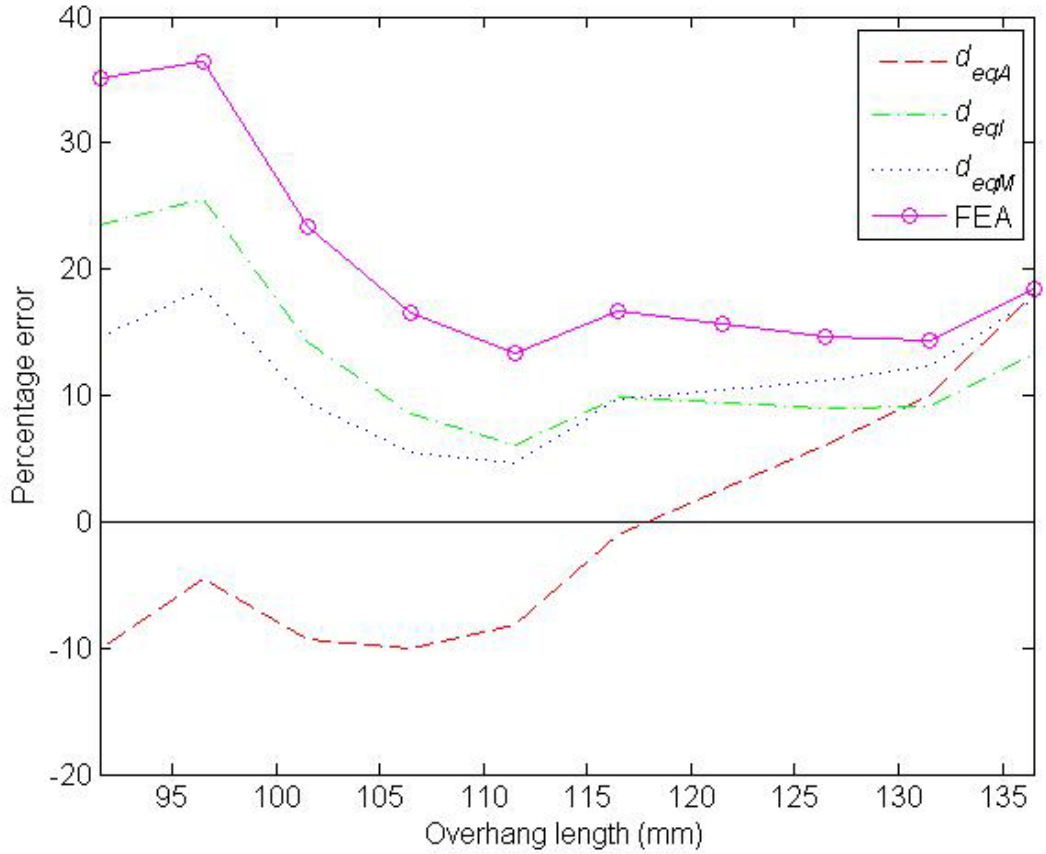

Figure 4-4. Normalized percentage error (average FEA mean error set to zero relative to experiment) for different equivalent diameters and FEA as a function of overhang length.

The new normalized natural frequency for each equivalent diameter was then compared to the FEA and experimental results. Table 4-5 shows the percentage difference between the mean error (including all overhang lengths) for the three equivalent diameter approaches and FEA.

Table 4-5. Comparison between the average error in natural frequency for each equivalent diameter over all overhang lengths relative to FEA/experiment.

Equivalent diameters	Percentage error
d_{eqI}	7.9
d_{eqM}	9.9
d_{eqA}	23.0

Tool Point Dynamics

The tool-collet holder assembly defined in Chapter 3 was modeled for six different overhang lengths of the tool (i.e., the length of the tool beyond the free end of the collet holder). The assembly receptances were also coupled to a rigid support. The purpose of this coupling was to identify the modes of the clamped-free tool-holder assembly and better understand their interactions with the spindle-machine modes. The measured receptances of the holder-spindle-machine (not including the tool) were also plotted. Finally, the measured and predicted receptances of the tool-holder-spindle-machine assembly were plotted to visualize the interactions between the spindle modes and tool-holder modes. The prediction of the tool point dynamics using different equivalent diameters was then compared to the experimental results.

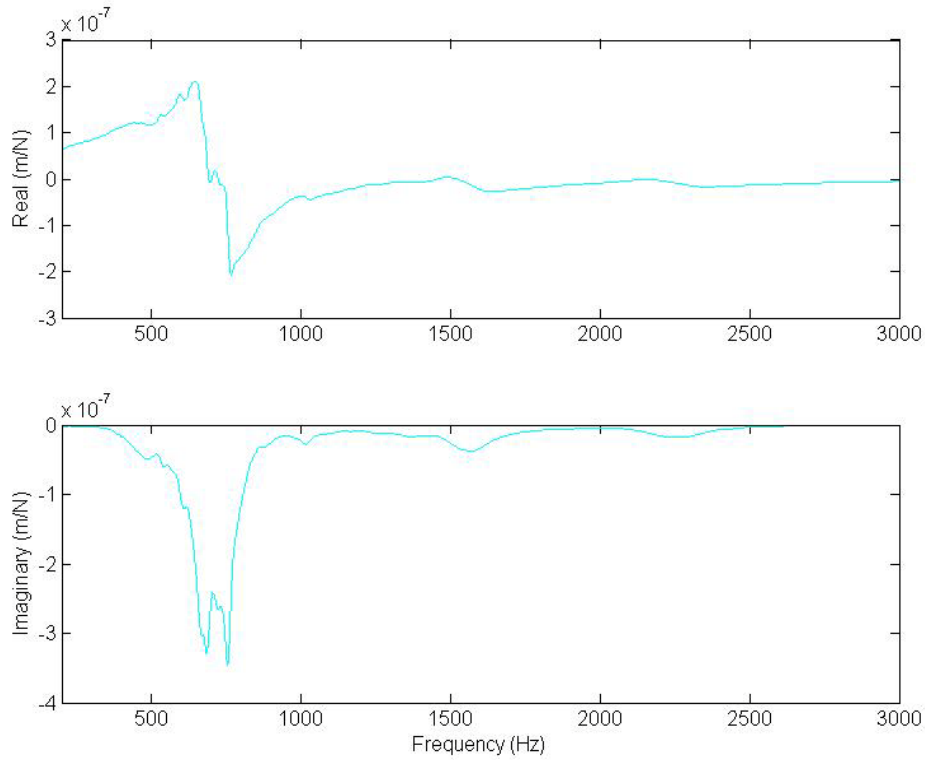

Figure 4-5. Measured direct FRF (H_{AA}) of the collet holder-spindle-machine.

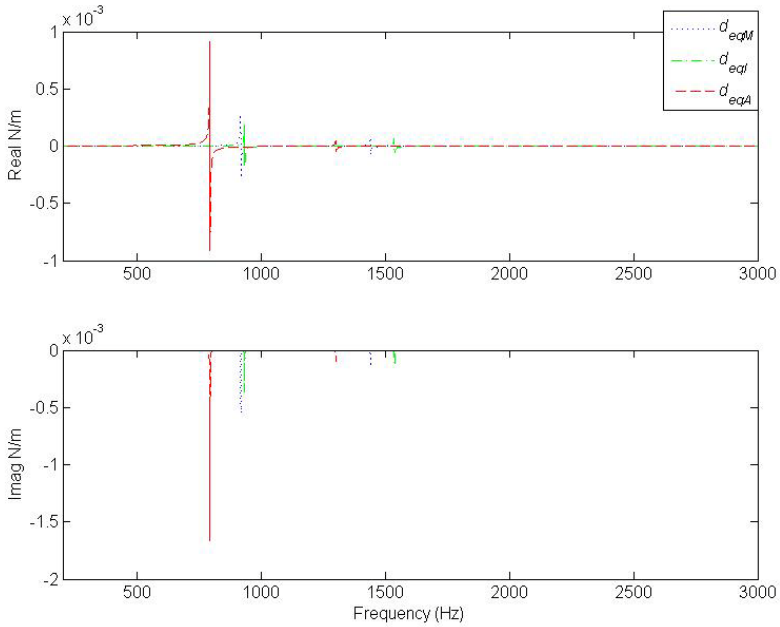

Figure 4-6. Clamped-free FRF of the modeled tool-holder substructure using different equivalent diameters. The tool overhang length is 86.5 mm. The first two bending modes are seen for each method.

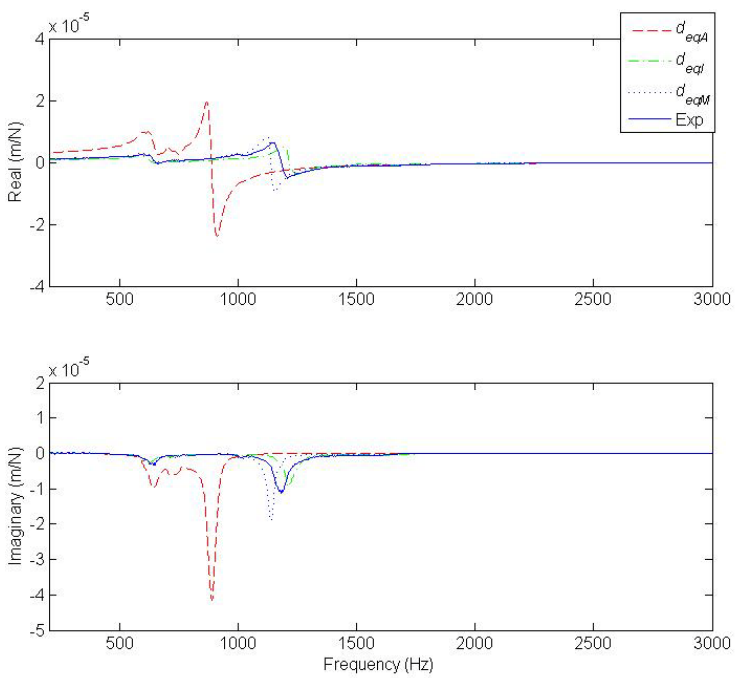

Figure 4-7. Measured (denoted as "Exp" in the legend) and predicted tool-holder-spindle direct FRFs (H_{11}) for three different equivalent diameters. The tool overhang length is 86.5 mm.

In Figure 4-5, the collet holder-spindle-machine direct FRF (at the subassembly's free end) is displayed. Multiple modes are evident with the lowest dynamic stiffness in the frequency range near 700 Hz.

By comparing Figures 4-5 and 4-6, the lower frequency mode in Figure 4-7 is identified as a spindle mode and the higher frequency mode as a tool-holder mode. Considering the higher frequency mode, the experimental results lie between the mass equivalent diameter approach (dotted line) and the moment of inertia equivalent diameter approach (dash-dot). The area-based equivalent diameter under predicts the natural frequency of the tool-holder substructure and, due to the natural frequency error, causes an incorrect interaction with the spindle-machine mode near 700 Hz.

For an overhang length of 96.5 mm (Figure 4-9), the experimental results show improved agreement with the mass equivalent diameter approach. The area-based prediction is again incorrect.

In Figure 4-11, the mass equivalent diameter approach captures the two peaks of the higher frequency mode, which indicates an interaction between the tool-holder mode and a spindle mode, and shows good agreement with the experimental results. The incorrect area-based trend continues.

From Figures 4-13, 4-15 and 4-17, it is seen that the reduction in natural frequency of the tool-holder substructure (with increasing tool overhang length) moves the interaction from a higher frequency spindle mode to the lower frequency spindle mode (near 700 Hz). Again, the area-based method offers the least prediction accuracy.

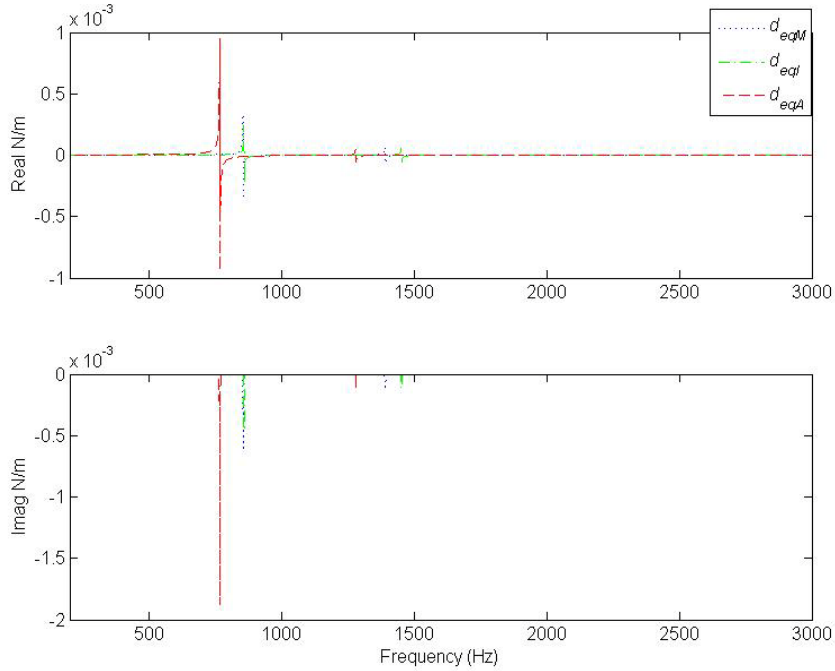

Figure 4-8. Clamped-free FRF of the modeled tool-holder substructure using different equivalent diameters. The overhang length is 96.5 mm.

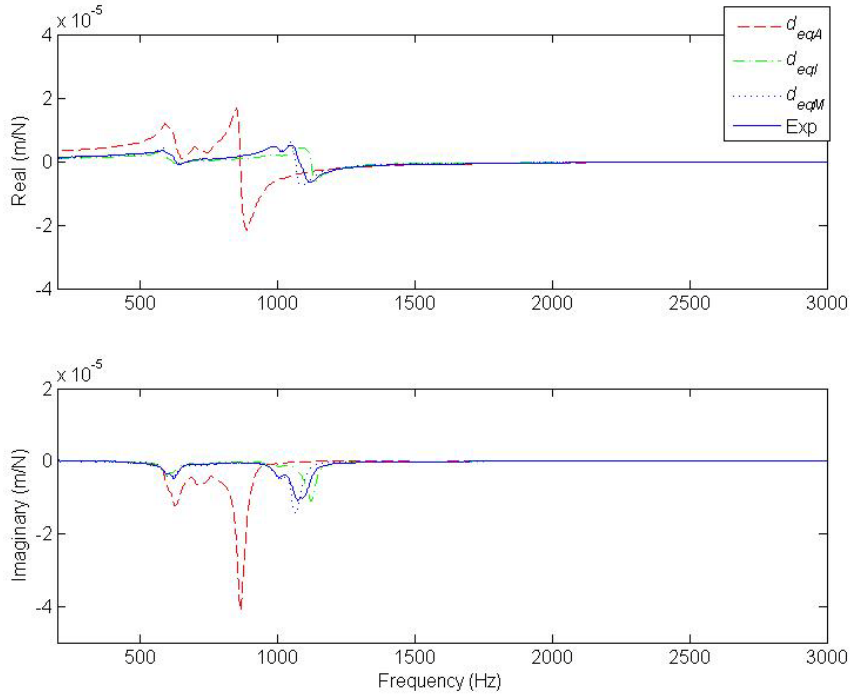

Figure 4-9. Measured and predicted tool-holder-spindle direct FRFs (H_{11}) for three different equivalent diameters. The tool overhang length is 96.5 mm.

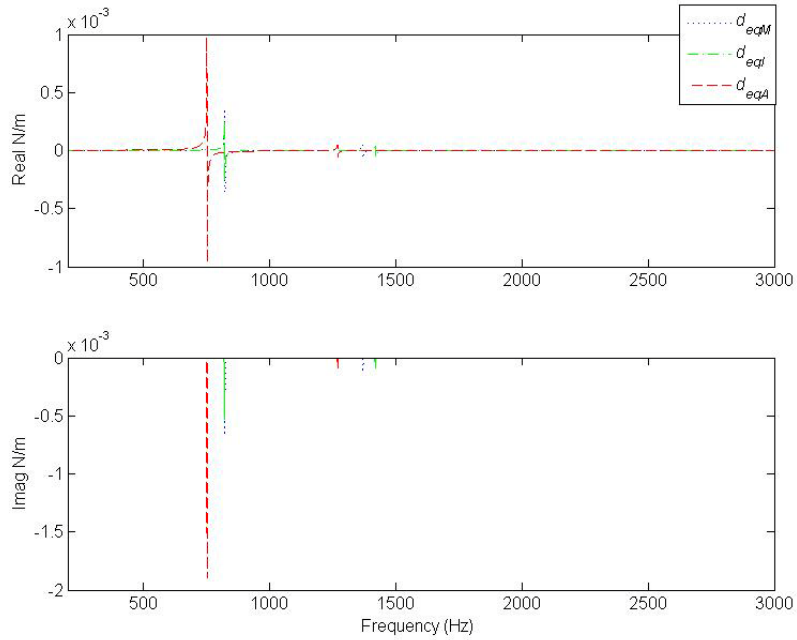

Figure 4-10. Clamped-free FRF of the modeled tool-holder substructure using different equivalent diameters. The overhang length is 101.5 mm.

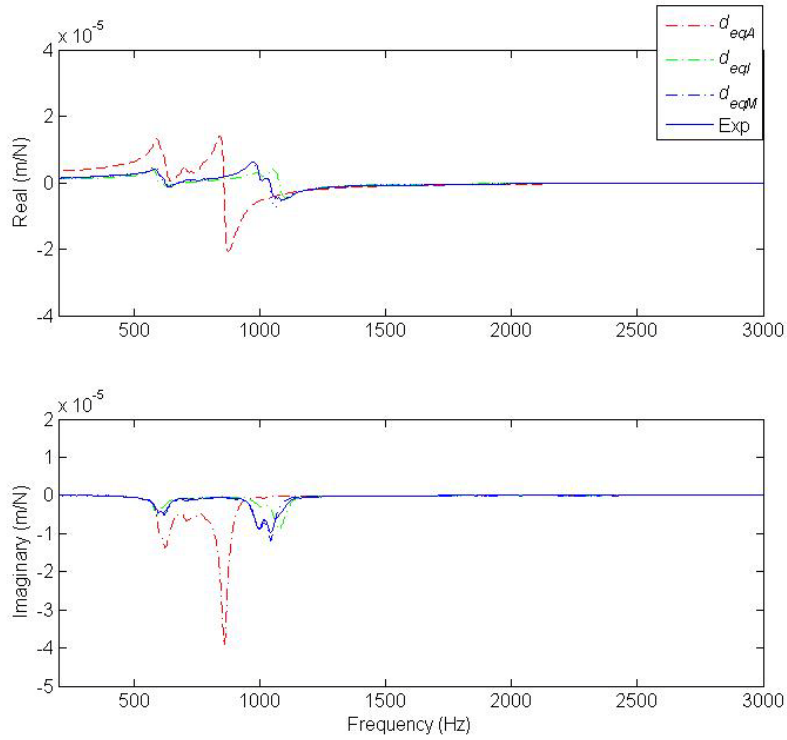

Figure 4-11. Measured and predicted tool-holder-spindle direct FRFs (H_{11}). The overhang length is 101.5 mm.

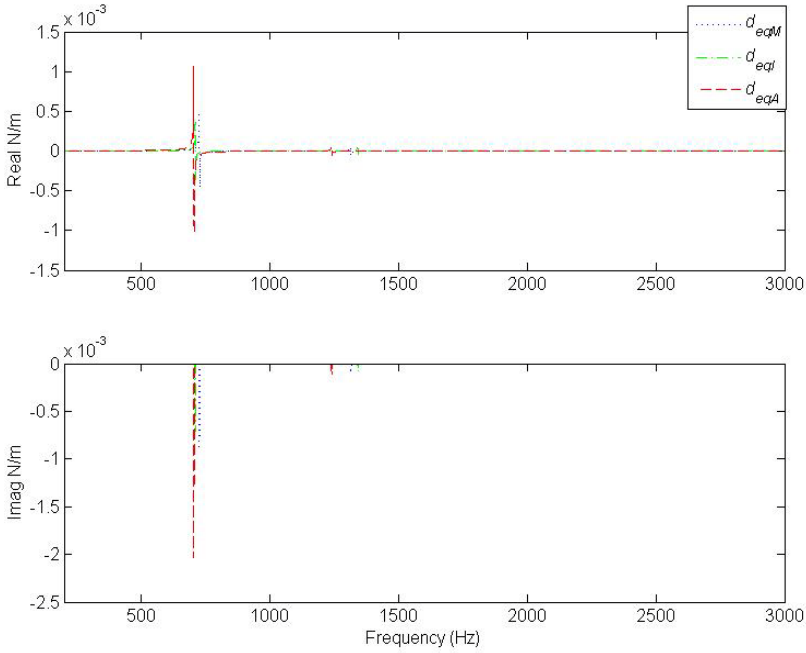

Figure 4-12. Clamped-free FRF of the modeled tool-holder substructure using different equivalent diameter. The overhang length is 116.5 mm.

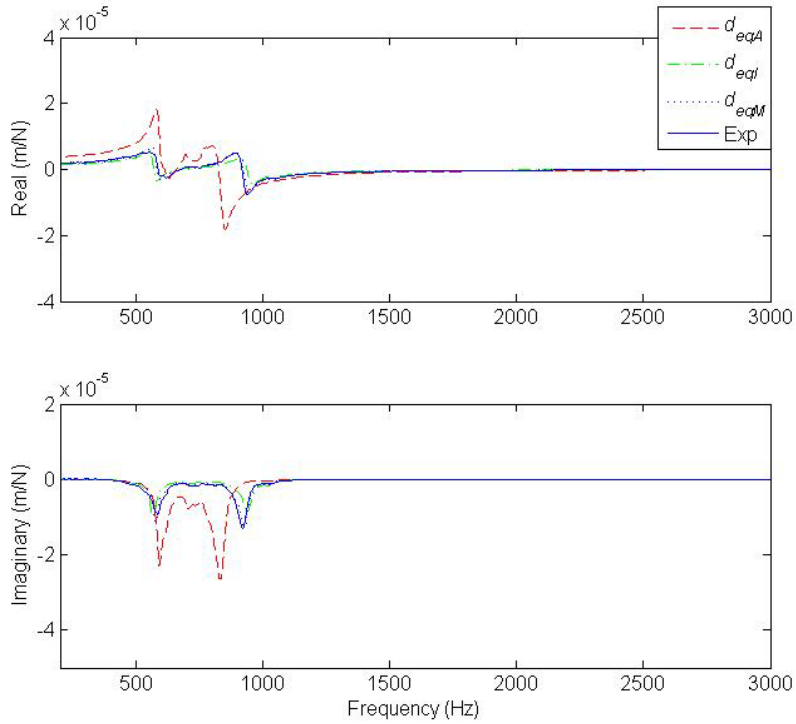

Figure 4-13. Measured and predicted tool-holder-spindle direct FRFs (H_{11}). The overhang length is 116.5 mm.

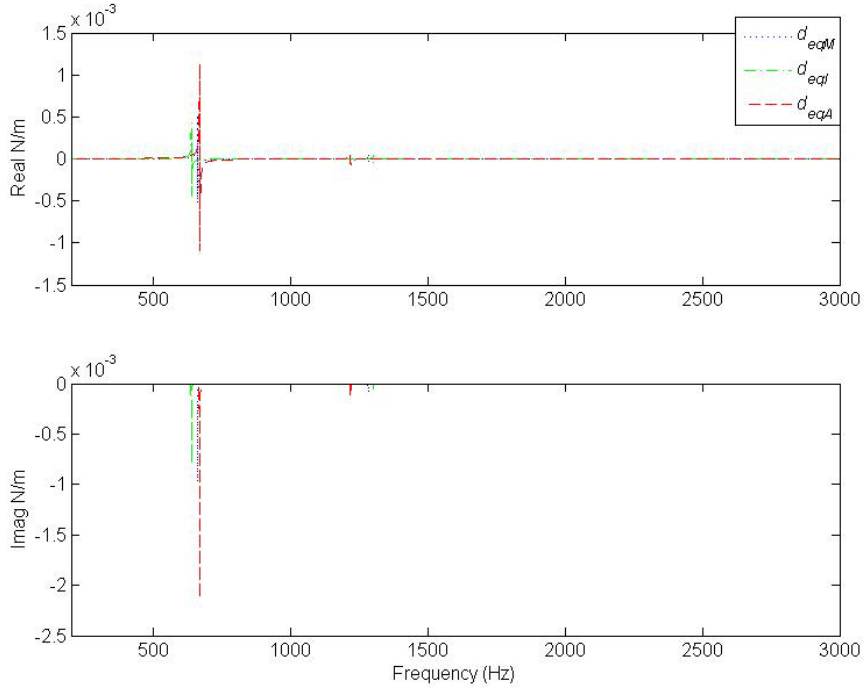

Figure 4-14. Clamped-free FRF of the modeled tool-holder substructure using different equivalent diameters. The overhang length is 126.5 mm.

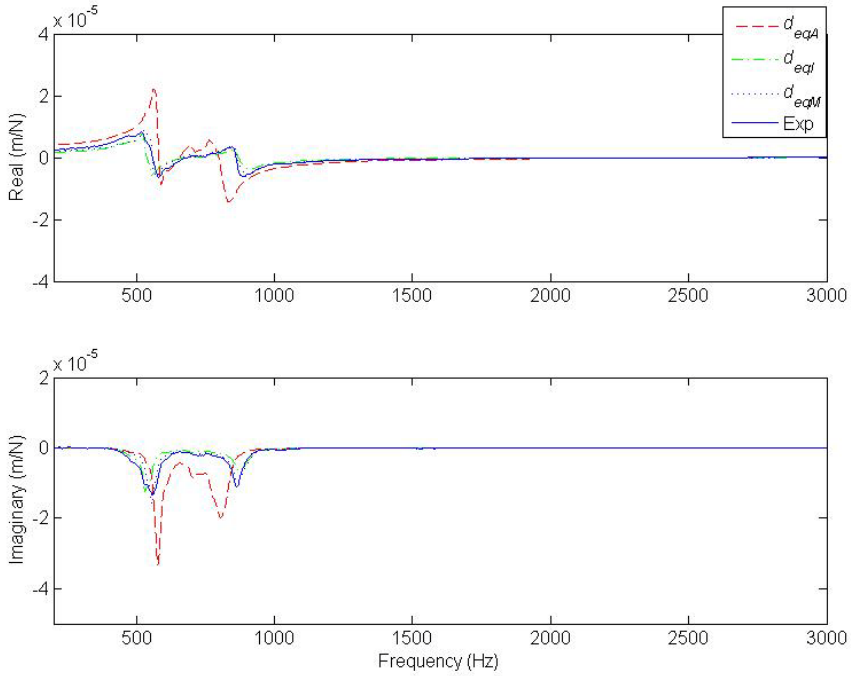

Figure 4-15. Measured and predicted tool-holder-spindle direct FRFs (H_{11}). The overhang length is 126.5 mm.

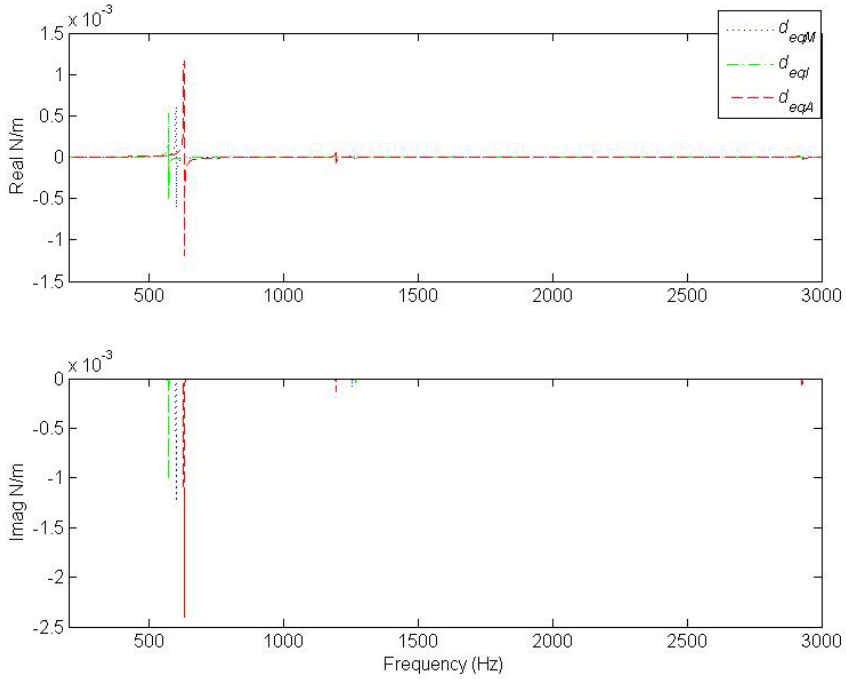

Figure 4-16. Clamped-free FRF of the modeled tool-holder substructure using different equivalent diameters. The overhang length is 136.5 mm.

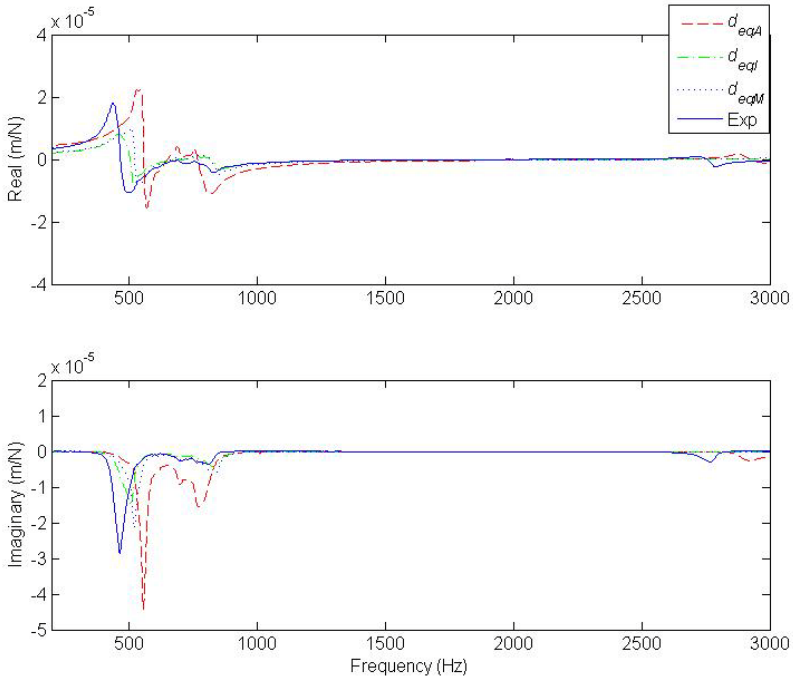

Figure 4-17. Measured and predicted tool-holder-spindle direct FRFs (H_{11}). The overhang length is 136.5 mm.

CHAPTER 5
CONCLUSION

Concluding Statements

The comparison between the natural frequencies obtained by FEA modal analysis and equivalent diameter model results for the clamped-free end mill, as well as modeled and experimental results for tool point dynamic responses (obtained using a selected collet holder-spindle-machine substructure), indicate that the "best" equivalent diameter for prediction accuracy varies with overhang lengths. Figure 4-4 shows that at lower overhang lengths, the prediction accuracy using the area moment of inertia method for equivalent diameter estimation (d_{eqI}) is highest, but as overhang length increases the response obtained by the mass-based equivalent diameter method (d_{eqM}) is more accurate. The results obtained using the area-based equivalent diameter (d_{eqA}) has a large percentage error with respect to FEA as compared to other methods (see Figure 4-4 and Table 4-5). The tool point FRF measurements and predictions also mimic the non-monotonic error behavior. The trend is further complicated by the inherent interactions between the tool-holder and spindle-machine modes. Though Figure 4-4 shows decreased percentage error for the area-based equivalent diameter (relative to FEA) as the overhang length increases, the tool-holder-spindle-machine assembly predictions and measurements completed here do not show good agreement for the selected overhang length range when using this method. This is partially the result of the complex interactions between the tool-holder and spindle-machine dynamics, which naturally vary from one machine to the next, even for the same tool-holder geometry.

Future Work

Future work should include calculation of the free-free receptances of the fluted portion of the tool over a range of 200 to 3000 Hz in ANSYS to compare the FEA-based receptances with

experimental results. Improvements in the three-dimensional tool model developed in Pro-E will also help in accurately determining the equivalent diameter calculation using area and moment of inertia. Better controlled clamped-free boundary conditions need to be provided in order to enable accurate validation data by experiments. Comparisons of the equivalent diameters and FEA approaches may also be made using a new approach in which the tool-holder model is developed using the spectral-Tchebychev technique to solve the Timoshenko beam equations (tool-holder assembly with different geometries and material properties are modeled individually and are combined analytically using component-mode synthesis technique) [20]. Additional experiments and predictions should also be completed on tools with various shank-to-flute length ratios coupled to other spindle-machine substructures and the three different equivalent diameter methods compared.

APPENDIX A
PROGRAM IN ANSYS PARAMETRIC DESIGN LANGUAGE (APDL)

```
! Calculation of h and n of beam!

/post1

/PNUM,NODE,1

m=200                    ! Number of intervals in the frequency range

! define the value of real and imag part of each node

*DIM,xrd1,,m

*DIM,xrd2,,m

*DIM,xrc1,,m

*DIM,xrc2,,m

*DIM,xid1,,m

*DIM,xid2,,m

*DIM,xic1,,m

*DIM,xic2,,m

*DIM,hrd,,m

*DIM,nrd,,m

*DIM,hrc,,m

*DIM,nrc,,m

*DIM,hid,,m

*DIM,nid,,m

*DIM,hic,,m

*DIM,nic,,m

*DIM,fre,,m
```

```
f=1.0                                  ! define the force/moment applied
*GET,yd1,NODE,75,LOC,Y                 ! get Y location of nodes for direct receptance
*GET,yd2,NODE,1074,LOC,Y
dyd=ABS(yd1-yd2)                       ! distance between two nodes
*GET,yc1,NODE,1278,LOC,Y               ! get Y location of nodes for cross receptance
*GET,yc2,NODE,8904,LOC,Y
dyc=ABS(yc1-yc2)                       ! distance between two nodes
*DO,n,1,m
  SET,1,n                              ! No. of substep
  *GET,fre(n),ACTIVE,0,SET,FREQ        ! get each step's frequency
  SET,1,n,1,0, , ,                     ! set the value of real part
  *GET,xrd1(n),NODE,75,U,X             ! real UX of node for direct receptance
  *GET,xrd2(n),NODE,1074,U,X
  hrd(n)=xrd1(n)/f                     ! real part of direct h
  nrd(n)=(xrd1(n)-xrd2(n))/(f*dyd)     ! real part of direct n
  *GET,xrc1(n),NODE,1278,U,X           ! real UX of NODE for cross receptance
  *GET,xrc2(n),NODE,8904,U,X
  hrc(n)=xrc1(n)/f                     ! real part of cross h
  nrc(n)=(xrc1(n)-xrc2(n))/(f*dyc)     ! real part of cross n
  SET,1,n,1,1, , ,                     ! set the value of imaginary part
  *GET,xid1(n),NODE,75,U,X             ! imag UX of node for direct receptance
  *GET,xid2(n),NODE,1074,U,X
  hid(n)=xid1(n)/f                     ! imag part of direct h
```

```
  nid(n)=(xid1(n)-xid2(n))/(f*dyd)      ! imag part of direct n
  *GET,xic1(n),NODE,1278,U,X       ! imag UX of node for cross receptance
  *GET,xic2(n),NODE,8904,U,X
  hic(n)=xic1(n)/f                          ! imag part of cross h
  nic(n)=(xic1(n)-xic2(n))/(f*dyc)      ! imag part of cross n
*ENDDO
*CFOPEN,H&N_by_force,xls
*VWRITE,
('direct and cross recptance of H and N')
*VWRITE,
('Freq','','HR_direct','  ','HI_direct','    ','NR_direct','  ','NI_direct','    ','HR_cross','   ','HI_cross','
          ','NR_cross','   ','NI_cross')
*VWRITE,fre(1),hrd(1),hid(1),nrd(1),nid(1),hrc(1),hic(1),nrc(1),nic(1)
(F5.1,'  ',F20.14,'        ',F20.14,'        ',F20.14,'        ',F20.14,'        ',F20.14,'        ',F20.14,'
          ',F20.14,'        ',F20.14)
*VWRITE,
('*******END********')
*CFCLOS
/PNUM,NODE,0
xrd1(1)=
xrd2(1)=
xrc1(1)=
xrc2(1)=
```

xid1(1)=

xid2(1)=

xic1(1)=

xic2(1)=

hrd(1)=

nrd(1)=

hrc(1)=

nrc(1)=

hid(1)=

nid(1)=

hic(1)=

nic(1)=

fre(1)=

FINI

APPENDIX B
MATLAB CODES

This section includes the MATLAB programs used to import the FEA Harmonic Analysis receptances from Excel files and then couple them to Timoshenko beam models.

Importing FEA Receptances

```
% FEA.m
% Uttara V Kumar
% Tony Schmitz
% Jun Zhang
% Program to read receptances stored in Excel from harmonic
% analysis in FEA



f = 200.1:0.1:600;        % Initializing frequency vector
f = f.';


% Import the receptance of the fluted portion calculated by
ANSYS
real_h66 = xlsread('H&N_by_force(200-600).xls',1,'B3:B4002');
imag_h66=xlsread('H&N_by_force(200-600).xls',1,'C3:C4002');
h66=(real_h66+i*imag_h66);

real_n66 = xlsread('H&N_by_force(200-600).xls',1,'D3:D4002');
imag_n66=xlsread('H&N_by_force(200-600).xls',1,'E3:E4002');
n66=(real_n66+i*imag_n66);

real_l66 = xlsread('L&P_by_moment(200-600).xls',1,'B3:B4002');
imag_l66=xlsread('L&P_by_moment(200-600).xls',1,'C3:C4002');
l66=(real_l66+i*imag_l66);

real_p66 = xlsread('L&P_by_moment(200-600).xls',1,'D3:D4002');
imag_p66=xlsread('L&P_by_moment(200-600).xls',1,'E3:E4002');
p66=(real_p66+i*imag_p66);

real_h67 = xlsread('H&N_by_force(200-600).xls',1,'F3:F4002');
imag_h67=xlsread('H&N_by_force(200-600).xls',1,'G3:G4002');
h67=(real_h67+i*imag_h67);

real_n67= xlsread('H&N_by_force(200-600).xls',1,'H3:H4002');
imag_n67=xlsread('H&N_by_force(200-600).xls',1,'I3:I4002');
n67=(real_n67+i*imag_n67);
```

```
real_l67 = xlsread('L&P_by_moment(200-600).xls',1,'F3:F4002');
imag_l67=xlsread('L&P_by_moment(200-600).xls',1,'G3:G4002');
l67=(real_l67+i*imag_l67);

real_p67 = xlsread('L&P_by_moment(200-600).xls',1,'H3:H4002');
imag_p67=xlsread('L&P_by_moment(200-600).xls',1,'I3:I4002');
p67=(real_p67+i*imag_p67);

n66 = l66;
n67 = -l67;

h77 = h66;
p77 = p66;

h76 = h67;
p76 = p67;

l77 = -l66;
n77 = l77;

l76 = -l67;
n76 = l67;

%  Define beam
d_out = 12.7e-3;                      % outer diameter, m
d_in  = 0;                            % inner diameter, m
lengths = 80e-3;                      % length of subcomponents, m
Eout =5.5e11;                         % modulus of holder, N/m^2
Ein = 5.5e11;                         % modulus of tool, N/m^2
densityout = 15000;                   % density of holder, kg/m^3
densityin = 15000;                    % density of tool, kg/m^3
eta = ones(1, length(d_out))*0.0015;% structural damping
Iout = pi/64*(d_out.^4-d_in.^4);      % second area moment of
                                        inertia for outer
                                        diameter, m^4
Iin = pi/64*(d_in.^4);                % second area moment of
                                        inertia for inner
                                        diameter, m^4
EIeq  = Eout.*Iout + Ein.*Iin;        % composite structural
                                        stiffness, N-m^2
EI = EIeq.*(1+i.*eta);                % damped structural
                                        stiffness, N-m^2
Aout = pi/4*(d_out.^2 - d_in.^2);     % cross-sectional area of
                                        outer diameter, m^2
Ain = pi/4*(d_in.^2);                 % cross-sectional area of
                                        inner diameter, m^2
```

```
m = lengths.*(Aout.*densityout + Ain.*densityin);% mass, kg

% Timoshenko terms
n = 50;                       % number of finite elements
nu_out = 0.22;                % Poisson's ratio of outer diameter
nu_in = 0.22;                 % Poisson's ratio of inner diameter
Gout = Eout./(2*(1+nu_out)); % shear modulus of outer diameter,
                                N/m^2
Gin = Ein./(2*(1+nu_in));    % shear modulus of inner diameter,
                                N/m^2
A = Aout + Ain;               % composite cross-sectional area,
                                m^2
AG = Gout.*Aout + Gin.*Ain;  % produce of area and shear modulus
                                For composite beam, N
nu = (nu_out.*Aout + nu_in.*Ain)./A; % composite Poisson's ratio
I = Iout + Iin;                      % composite second area
                                       moment of inertia, m^4
rg = (I./A).^0.5;                    % radius of gyration, m
mpl = densityout.*Aout + densityin.*Ain;  % mass per unit
length, kg/m

for cnt = 1:length(d_in)
    if (d_in(cnt) == 0) | ((d_in(cnt) ~= 0) & (Ein(cnt) ~= 0))
% solid cross-section
        kp(cnt) = 6*(1+nu(cnt))^2/(7+12*nu(cnt)+4*nu(cnt)^2);
% shape factor
    else      % hollow cross-section
        num = 6*(1 + nu_out(cnt))^2*(d_in(cnt)^2 +
d_out(cnt)^2)^2;
        den = 7*d_in(cnt)^4 + 34*d_in(cnt)^2*d_out(cnt)^2 +
7*d_out(cnt)^4 + nu_out(cnt)*(12*d_in(cnt)^4 +
48*d_in(cnt)^2*d_out(cnt)^2 + 12*d_out(cnt)^4) +
nu_out(cnt)^2*(4*d_in(cnt)^4 + 16*d_in(cnt)^2*d_out(cnt)^2 +
4*d_out(cnt)^4);
        kp(cnt) = num/den;
    end
    cnt
end

% Determine free-free receptance of beam
% h = x/f
% l = x/m
% n = theta/f
% p = theta/m
[h33, l33, n33, p33, h44, l44, n44, p44, h34, l34, n34, p34,
h43, l43, n43, p43] = timo_free_free(f, EI(1), lengths(1),
AG(1), kp(1), rg(1), mpl(1), n);
```

```
[h66, l66, n66, p66, h77, l77, n77, p77, h67, l67, n67, p67,
h76, l76, n76, p76] = couple_free_free(f, h66, l66, n66,...
    p66, h77, l77, n77, p77, h67, l67, n67, p67, h76, l76, n76,
p76, h33, l33, n33, p33, h44, l44, n44, p44, h34, l34,...
    n34, p34, h43, l43, n43, p43);

% Rigid support receptances
h55 = zeros(size(h33));
l55 = zeros(size(h33));
n55 = zeros(size(h33));
p55 = zeros(size(h33));

%Coupling free-free beam receptances to rigid wall
[H11 L11 N11 P11] = Couple_forward2(f,h66, l66, n66, p66, h77,
l77, n77, p77, h67, l67,...
    n67, p67, h76, l76, n76, p76, h55, l55, n55, p55);

%Plot figure
figure(1)
subplot(211)
plot(f, real(H11), 'm--')
set(gca, 'FontSize', 12)
xlim([200 600])
ylabel('Real (m/N)')
hold on
subplot(212)
plot(f, imag(H11), 'm--')
set(gca, 'FontSize', 12)
xlim([200 600])
xlabel('Frequency (Hz)')
ylabel('Imaginary (m/N)')
hold on
```

Free-Free Beam Receptances

```
% timo_free_free.m
% T. Schmitz (8/20/04)
% This program uses n Timoshenko beam elements to determine end
receptances for free-free beam.
% Input variables are: f, frequency, Hz; EI, structural rigidity
including hysteretic damping, N-m^2;% L, beam length, m;
% density, kg/m^3; A, cross sectional area, m^2; kp, shear
factor; G, shear modulus, N/m^2;
% rg, radius of gyration; n, number of elements
```

```
function [h11, l11, n11, p11, h22, l22, n22, p22, h12, l12, n12,
p12, h21, l21, n21, p21] = timo_free_free(f, EI, L, AG, kp, rg,
mpl, n);
l = L/n;                    % length of each finite element, m
phi = 12*EI/(kp*AG*l^2);    % shear deformation parameter

% Single element matrices for Timoshenko beam
% Mass matrix
Mt = mpl*l/(1+phi)^2*[(13/35+7*phi/10+phi^2/3)
(11/210+11*phi/120+phi^2/24)*l (9/70+3*phi/10+phi^2/6) -
(13/420+3*phi/40+phi^2/24)*l;
    (11/210+11*phi/120+phi^2/24)*l (1/105+phi/60+phi^2/120)*l^2
(13/420+3*phi/40+phi^2/24)*l -(1/140+phi/60+phi^2/120)*l^2;
    (9/70+3*phi/10+phi^2/6) (13/420+3*phi/40+phi^2/24)*l
(13/35+7*phi/10+phi^2/3) -(11/210+11*phi/120+phi^2/24)*l;
    -(13/420+3*phi/40+phi^2/24)*l -(1/140+phi/60+phi^2/120)*l^2
-(11/210+11*phi/120+phi^2/24)*l (1/105+phi/60+phi^2/120)*l^2];
Mr = mpl*l/(1+phi)^2*(rg/l)^2*[6/5 (1/10-phi/2)*l -6/5 (1/10-
phi/2)*l;
    (1/10-phi/2)*l (2/15+phi/6+phi^2/3)*l^2 -(1/10-phi/2)*l -
(1/30+phi/6-phi^2/6)*l^2;
    -6/5 -(1/10-phi/2)*l 6/5 -(1/10-phi/2)*l;
    (1/10-phi/2)*l -(1/30+phi/6-phi^2/6)*l^2 -(1/10-phi/2)*l
(2/15+phi/6+phi^2/3)*l^2];
M = Mt + Mr;

% Stiffness matrix
Kb = EI/(l^3*(1+phi)^2)*[12 6*l -12 6*l;
    6*l (4+2*phi+phi^2)*l^2 -6*l (2-2*phi-phi^2)*l^2;
    -12 -6*l 12 -6*l;
    6*l (2-2*phi-phi^2)*l^2 -6*l (4+2*phi+phi^2)*l^2];
Ks = kp*AG*phi^2/(4*l*(1+phi)^2)*[4 2*l -4 2*l;
    2*l l^2 -2*l l^2;
    -4 -2*l 4 -2*l;
    2*l l^2 -2*l l^2];
K = Kb + Ks;

Mtemp2 = M;
Ktemp2 = K;

% Build full mass and stiffness matrices
for cnt = 2:n
    % Concatenate left element matrices with required zeros
    right = zeros(cnt*2, 2);
    bottom = zeros(2, (cnt+1)*2);

    % Mass matrix
```

```
    temp = cat(2, M, right);
    Mtemp1 = cat(1, temp, bottom);

    % Stiffness matrix
    temp = cat(2, K, right);
    Ktemp1 = cat(1, temp, bottom);

    % Concatenate right element matrices with required zeros
    left = zeros(cnt*2, 2);
    top = zeros(2, (cnt+1)*2);

    % Mass matrix
    temp = cat(2, left, Mtemp2);
    Mtemp2 = cat(1, top, temp);

    % Stiffness matrix
    temp = cat(2, left, Ktemp2);
    Ktemp2 = cat(1, top, temp);

    % Add two matrices
    M = Mtemp1 + Mtemp2;
    K = Ktemp1 + Ktemp2;
end

% Calculate required direct and cross receptances for ends of
beam
for cnt = 1:length(f)
    w = f(cnt)*2*pi;        % frequency, rad/s
    D = inv(-M*w^2 + K);    % dynamic matrix
    h11(cnt) = D(1,1);
    l11(cnt) = -D(1,2);
    n11(cnt) = -D(2,1);
    p11(cnt) = D(2,2);

    h12(cnt) = D(1,2*(n+1)-1);
    l12(cnt) = -D(1,2*(n+1));
    n12(cnt) = -D(2,2*(n+1)-1);
    p12(cnt) = D(2,2*(n+1));

    h21(cnt) = D(2*(n+1)-1,1);
    l21(cnt) = -D(2*(n+1)-1,2);
    n21(cnt) = -D(2*(n+1),1);
    p21(cnt) = D(2*(n+1),2);

    h22(cnt) = D(2*(n+1)-1,2*(n+1)-1);
    l22(cnt) = -D(2*(n+1)-1,2*(n+1));
    n22(cnt) = -D(2*(n+1),2*(n+1)-1);
```

```
    p22(cnt) = D(2*(n+1),2*(n+1));

    clear D;
end
```

Coupling Free-Free Beam Receptances

```
% T. Schmitz and Gregory Duncan
% Couple_free_free.m
% Function used to couple two free-free beams.

function [h11, l11, n11, p11, h44, l44, n44, p44, h14, l14, n14,
p14, h41, l41, n41, p41] = couple_free_free(f, h11, l11, n11,
p11,...
          h22, l22, n22, p22, h12, l12, n12, p12, h21, l21, n21,
p21, h33, l33, n33, p33, h44, l44, n44, p44, h34, l34, n34,
p34,...
          h43, l43, n43, p43);

[N col] = size(f);

h11=reshape(h11,1,1,N);
l11=reshape(l11,1,1,N);
n11=reshape(n11,1,1,N);
p11=reshape(p11,1,1,N);

h12=reshape(h12,1,1,N);
l12=reshape(l12,1,1,N);
n12=reshape(n12,1,1,N);
p12=reshape(p12,1,1,N);

h21=reshape(h21,1,1,N);
l21=reshape(l21,1,1,N);
n21=reshape(n21,1,1,N);
p21=reshape(p21,1,1,N);

h22=reshape(h22,1,1,N);
l22=reshape(l22,1,1,N);
n22=reshape(n22,1,1,N);
p22=reshape(p22,1,1,N);

h33=reshape(h33,1,1,N);
l33=reshape(l33,1,1,N);
n33=reshape(n33,1,1,N);
p33=reshape(p33,1,1,N);
```

```
h34=reshape(h34,1,1,N);
l34=reshape(l34,1,1,N);
n34=reshape(n34,1,1,N);
p34=reshape(p34,1,1,N);

h43=reshape(h43,1,1,N);
l43=reshape(l43,1,1,N);
n43=reshape(n43,1,1,N);
p43=reshape(p43,1,1,N);

h44=reshape(h44,1,1,N);
l44=reshape(l44,1,1,N);
n44=reshape(n44,1,1,N);
p44=reshape(p44,1,1,N);

RS11 = [h11 l11; n11 p11];
RS12 = [h12 l12; n12 p12];
RS21 = [h21 l21; n21 p21];
RS22 = [h22 l22; n22 p22];

RS33 = [h33 l33; n33 p33];
RS34 = [h34 l34; n34 p34];
RS43 = [h43 l43; n43 p43];
RS44 = [h44 l44; n44 p44];

R11=zeros(2,2,N);
R41=zeros(2,2,N);
R14=zeros(2,2,N);
R44=zeros(2,2,N);

for n=1:N
    R11(:,:,n) = RS11(:,:,n) -
RS12(:,:,n)*((RS22(:,:,n)+RS33(:,:,n))\RS21(:,:,n));
    R41(:,:,n) =
RS43(:,:,n)*((RS22(:,:,n)+RS33(:,:,n))\RS21(:,:,n));
    R14(:,:,n) =
RS12(:,:,n)*((RS22(:,:,n)+RS33(:,:,n))\RS34(:,:,n));
    R44(:,:,n) = RS44(:,:,n) -
RS43(:,:,n)*((RS22(:,:,n)+RS33(:,:,n))\RS34(:,:,n));
end

h11 = R11(1,1,:);
l11 = R11(1,2,:);
n11 = R11(2,1,:);
p11 = R11(2,2,:);

h14 = R14(1,1,:);
```

```
l14 = R14(1,2,:);
n14 = R14(2,1,:);
p14 = R14(2,2,:);

h41 = R41(1,1,:);
l41 = R41(1,2,:);
n41 = R41(2,1,:);
p41 = R41(2,2,:);

h44 = R44(1,1,:);
l44 = R44(1,2,:);
n44 = R44(2,1,:);
p44 = R44(2,2,:);

h11=reshape(h11,1,N);
l11=reshape(l11,1,N);
n11=reshape(n11,1,N);
p11=reshape(p11,1,N);

h14=reshape(h14,1,N);
l14=reshape(l14,1,N);
n14=reshape(n14,1,N);
p14=reshape(p14,1,N);

h41=reshape(h41,1,N);
l41=reshape(l41,1,N);
n41=reshape(n41,1,N);
p41=reshape(p41,1,N);

h44=reshape(h44,1,N);
l44=reshape(l44,1,N);
n44=reshape(n44,1,N);
p44=reshape(p44,1,N);
```

Coupling Free-Free Section to a Cantilevered Section

```
% Couple_forward2.m
% Scott Duncan
% Program to couple in a forward direction based on a free-free
section attached to a cantilevered section, finding output at
end of attached
% free-free Coordinate system  3 -- 2 - 1

% Inputs (f, h11, l11, n11, p11, h22, l22, n22, p22, h12, l12,
n12, p12, h21, l21, n21, p21)
```

```
%  Outputs ( H11, L11, N11, P11)

function [H11, L11, N11, P11] = Couple_forward2(f, h11, l11,
n11, p11, h22, l22, n22, p22, h12, l12, n12, p12, h21, l21, n21,
p21, h33, l33, n33, p33)

N=length(f);

%%reshape vectors to assemble 3D matrices
h11=reshape(h11,1,1,N);
l11=reshape(l11,1,1,N);
n11=reshape(n11,1,1,N);
p11=reshape(p11,1,1,N);

h22=reshape(h22,1,1,N);
l22=reshape(l22,1,1,N);
n22=reshape(n22,1,1,N);
p22=reshape(p22,1,1,N);

h12=reshape(h12,1,1,N);
l12=reshape(l12,1,1,N);
n12=reshape(n12,1,1,N);
p12=reshape(p12,1,1,N);

h21=reshape(h21,1,1,N);
l21=reshape(l21,1,1,N);
n21=reshape(n21,1,1,N);
p21=reshape(p21,1,1,N);

h33=reshape(h33,1,1,N);
l33=reshape(l33,1,1,N);
n33=reshape(n33,1,1,N);
p33=reshape(p33,1,1,N);

%%Assemble matrices size 2X2XN
R21 = [h21 l21; n21 p21];
R12 = [h12 l12; n12 p12];
R22 = [h22 l22; n22 p22];
R11 = [h11 l11; n11 p11];
R33 = [h33 l33; n33 p33];

%%predefine G11f matrix for for loop
G11f=zeros(2,2,N);

for n=1:N
    G11(:,:,n) = R11(:,:,n) -
R12(:,:,n)*((R22(:,:,n)+R33(:,:,n))\R21(:,:,n));
```

```
end

H11 = G11(1,1,:);
L11 = G11(1,2,:);
N11 = G11(2,1,:);
P11 = G11(2,2,:);

H11=reshape(H11,1,N);
L11=reshape(L11,1,N);
N11=reshape(N11,1,N);
P11=reshape(P11,1,N);
```

LIST OF REFERENCES

1. J. Tlusty, Manufacturing Processes and Equipment, Prentice Hall, Upper Saddle River, NJ, 1999.

2. Y. Altintas, Manufacturing Automation, Cambridge University Press, UK, 2000.

3. T. L. Schmitz, K.S. Smith, Machining Dynamics: Frequency Response to Improved Productivity, Springer, NY, 2009.

4. T. Schmitz, R.R. Donaldson, Predicting high-speed machining dynamics by substructure analysis, Annals of the CIRP 49 (1) (2000) 303-308.

5. L. Kops, D. Vo, Determination of the equivalent diameter of an end mill based on its compliance, Annals of the CIRP 39 (1) (1990) 93-96.

6. T. Schmitz, G.S. Duncan, Three-component receptance coupling substructure analysis for tool point dynamics prediction, Journal of Manufacturing Science and Engineering 127 (4) (2005) 781-790.

7. T. Schmitz, K. Powell, D. Won, G.S. Duncan, W.G. Sawyer, J. Ziegert, Shrink fit tool holder connection stiffness/damping modeling for frequency response prediction in milling, International Journal of Machine Tools and Manufacture 47 (9) (2007) 1368-1380.

8. S. Smith, J. Tlusty, An overview of modeling and simulation of the milling process, Journal of Engineering for Industry, Transactions of the ASME 113 (1991) 169-175.

9. R. E. Devor, W.A. Kline, W.J. Zdeblick, A mechanistic model for the force system in end milling with application to machining airframe structures, Transactions of the NAMRI/SME 18 (1980) 297-303.

10. J. Tlusty, W. Zaton, F. Ismail, Stability lobes in milling, Annals of the CIRP 32 (1) (1983) 309-313.

11. Y. Altintas, E. Budak, Analytical prediction of stability lobes in milling, Annals of the CIRP 44 (1) (1995) 357-362.

12. T. Schmitz, B. Mann, Closed form solutions for surface location error in milling, International Journal of Machine Tools and Manufacture 46 (2006) 1369-1377.

13. T. Insperger, G. Stépán, Semi-discretization method for delayed systems, International Journal for Numerical Methods in Engineering 55 (5) (2002) 503-518.

14. I. Deiab, S. Veldhuis, M. Dumitrescu, Dynamic modeling of face milling process including the effect of fixture dynamics, Transactions of the NAMRI/SME V 30 (2002) 461-468.

15. B. Mann, P. Bayly, M. Davies, J. Halley, Limit cycles, bifurcations, and accuracy of the milling process, Journal of Sound and Vibration 227 (2004) 31-48.

16. R. E. D. Bishop, D.C. Johnson, The Mechanics of Vibration, Cambridge University Press, Cambridge, UK, 1960.

17. S. Park, Y. Altintas, M. Movahhedy, Receptance coupling for end mills, International Journal of Machine Tools and Manufacture 43 (2003) 889-896.

18. E. B. Kivanc, E. Budak, Structural modeling of end mills for form error and stability analysis, International Journal of Machine Tools and Manufacture 44 (2004) 1151-1161.

19. A. Ertürk, H.N. Özgüven, E. Budak, Analytical modeling of spindle–tool dynamics on machine tools using timoshenko beam model and receptance coupling for the prediction of tool point FRF, International Journal of Machine Tools and Manufacture 46 (15) (2006) 1901-1912.

20. S. Filiz, C.-H. Cheng, K. Powell, T. Schmitz, O.B. Ozdoganlar, An improved tool-holder model for RCSA tool-point frequency response prediction, Precision Engineering 33 (1) (2009) 26-36.

21. W. Weaver Jr., S. Timoshenko, D. Young, Vibration Problems in Engineering, 5th Ed., John Wiley and Sons, New York, NY, Section 5.12.

22. S. Sattinger, A method for experimentally determining rotational mobilities of structures, Shock and Vibration Bulletin 50 (1980) 17-27.

23. D.J. Ewins, Modal Testing: Theory, Practice and Applications, 2nd Edition, Research Studies Press, 2000.

24. G. S. Duncan, Milling dynamics prediction and uncertainty analysis using receptance coupling substructure analysis, PhD Dissertation, University of Florida, 2006.

BIOGRAPHICAL SKETCH

Uttara Vijay Kumar was born and raised in New Delhi, the capital city of India. She received her Bachelor of Technology degree in mechanical and automation engineering from Indira Gandhi Institute of Technology, a constituent college of Guru Gobind Singh Indraprastha University, Delhi in May 2007. In fall 2007 she began her graduate studies at the Department of Mechanical and Aerospace Engineering, University of Florida, in pursuit of her MS degree in mechanical engineering. In spring 2008, she joined the Machine Tool Research Center under the guidance of Dr. Tony L. Schmitz.